ABSTRACT

KHAN, MOHAMMAD RASHED. Engineering the Yield Properties of the Oxide Skin on a Liquid Metal Alloy. (Under the direction of Michael D. Dickey.)

The aim of this thesis is to study, control, and manipulate the properties of a passivating surface oxide layer (skin) that forms spontaneously at ambient temperature on a room temperature liquid metal alloy, eutectic gallium indium (EGaIn). The oxide skin governs the electrical, mechanical, and chemical properties of the surface of the metal. We demonstrate the utility of this skin by creating reconfigurable electronics (e.g., antenna and microstrip filter) that change shape by flow. The ability to flow and stabilize the liquid metal on demand for shaping it into useful and responsive structures (e.g., antennas, switches, sensors, electronic filters) relies on the rupture and reformation of the oxide skin. We seek to understand these properties to better control the shape of the metal.

Rheology and electrochemistry provide fundamental and quantitative information about the behavior of this skin under various mechanical and chemical environments. In a stress controlled rheometer, parallel plates sandwich EGaIn and measure the modulus and yield stress of the skin by oscillatory stress-strain measurements. The mechanical properties of EGaIn on the micro scale can be tuned by modifying the skin. A home built chamber on the rheometer controls the chemical environment surrounding the metal (e.g., water, aqueous solutions, and organic solvents) and allows for the measurement of the modified mechanical properties of the interface of EGaIn in these environments. The results suggest that certain environments (water, acid) weaken the skin and others (polyvinylalcohol) reinforce the skin.

To detect the real time oxidation and rupture of the oxide layer, we utilize an amperometric technique. We hypothesized that electrochemical measurements could detect the oxidation of freshly exposed metal. We describe a new amperometric technique for measuring the oxidization of metal that takes advantage of the liquid nature of EGaIn. We utilize EGaIn as a working electrode and expel the metal out of a syringe at a controlled flow rate to create new surface area at a known rate. As the EGaIn droplet enlarges, the skin ruptures and oxidation ensues. We measure and analyze the amperometric signals arising from this technique. This work is a first step toward ultimately integrating electrochemistry with rheology in a novel manner so as to elucidate the rupture of the oxide skin under controlled mechanical conditions (i.e., in the rheometer) and correlate the resulting changes in mechanical properties in real time.

# Engineering the Yield Properties of the Oxide Skin on a Liquid Metal Alloy

by
Mohammad Rashed Khan

A thesis submitted to the Graduate Faculty of
North Carolina State University
in partial fulfillment of the
requirements for the Degree of
Master of Science

Chemical Engineering

Raleigh, North Carolina

2011

APPROVED BY:

| | |
|---|---|
| _____ | _____ |
| Michael Dickey<br>(Committee Chair) | Edmond F. Bowden |
| _____ | |
| Richard Spontak | |

# BIOGRAPHY

Mohammad Rashed Khan was born on August 23, 1983, in Dhaka, Bangladesh. He grew up in Dhaka, Bangladesh as well. After graduating from Dhaka Residential Model College in August, 2000, he entered into Bangladesh University of Engineering and Technology (BUET) for his undergraduate degree in Chemical Engineering. In 2007, he graduated with his Bachelor of Science in Chemical Engineering from BUET. He worked as a Lecturer in the same department of BUET for 2 years. In fall 2009, he joined in the Department of Chemical and Biomolecular engineering at NC State University as a graduate student.

# ACKNOWLEDGEMENTS

First and foremost, I would like to express my gratitude to my advisor, Dr.Michael Dickey, for his constant guidance, encouragement, and patience. It has been an honor to learn from him. I would also like to thank Dr. Richard Spontak and Dr. Edmond Bowden to be a part of my committee members.

I would like to thank Dr. Peter Fedkiw, Dr. Aulice Scibioh for their helpful discussion regarding electrochemistry measurements; Christina Tang and Dr. Chris Bonino for their help with Rheometer, and Kit Yeung for his support in maintaining Rheometer and Recirculator.

My appreciation also goes to the lab members in the Dickey research group- particularly, Ju-Hee So, to help me get trained in lab. Ju-Hee So and I have worked together for the fundamental studies of the liquid metal; Berc Kalanyan, to setup the electrochemical cell; Gerard Hayes for Reconfigurable antenna characterization; Silu Zhang for her hard work to finish microstrip filter project; Sharvil Desai for his constant support during my experiments; Jacob Thelen and Dr. Thomas Ward for the high speed camera. Jacob also deserves special thanks for some nice pictures. Last but not the least, the undergrads who worked with me in different times to produce some nice work- particularly Justin, John, Jennifer, Nathan, Jarrett. It was my pleasure mentor them. It was also fun to train a lot of graduate students and undergraduate students in the lab. Finally, I would like to thank my parents, uncle, sister and specially Taliman, my wife, for their constant love and support in every single moment of my life. I would also like to thank almighty Allah for everything else.

# TABLE OF CONTENTS

# LIST OF FIGURES

**Chapter 2**



**Chapter 3**



**Chapter 4**

**Chapter 5**

# CHAPTER 1

## 1.1 Research Focus

The aim of this thesis is to study, control, and manipulate the properties of a passivating[1] surface oxide layer (skin) that forms spontaneously at ambient temperature on a room temperature liquid metal alloy, eutectic gallium indium[2] (EGaIn). The skin provides mechanical stability to the high surface tension[3,4], low viscosity[5] liquid metal such that it can be molded into useful shapes (e.g., antennas[6-10], interconnects[11,12], self assembled monolayer[13,14] and electrodes[15]). Rupturing the skin allows it to flow (e.g., into microfluidic channels to define its shape) and provides a method to create conductive structures that change shape, and therefore function, in response to stimuli. We seek to understand these properties to better control the shape of the metal. Rheology and electrochemistry provide quantitative information about the behavior of this skin under various mechanical and chemical environments. These fundamental studies provide the basis for the design of soft, functional structures that harness these properties using microfluidics. We aim to accomplish the following in this study:

1. **Fabrication of shape shifting devices** (e.g., a reconfigurable antenna and fluidic filter) by using engineered microfluidic channels that harness the rheological and yield properties of EGaIn. **Study of the rheological properties of EGaIn**. The unusual properties of EGaIn arise primarily from its skin. Rheological

characterization of the skin quantifies the yield properties as a function of processing of the metal and the chemical environment surrounding the skin. Understanding these changes is important for controlling and tuning the response of the metal to pressure in microfluidic devices.

2. **Study of the oxidation of EGaIn**. The goal is to use electrochemistry to detect and measure both the formation and rupture of the oxide layer. When the oxide skin yields, the underlying metal becomes exposed and oxidizes. We seek to measure and understand these events.

## 1.2 Introduction

Eutectic gallium indium (EGaIn[2], Gallium 75 wt% and Indium 25 wt%) is a gallium-rich liquid metal alloy with low viscosity[5] and high conductivity[3]. It forms spontaneously an oxide skin[1,5] at room temperature. The presence of this oxide skin enables this low viscosity alloy to be micromolded into stable, non-spherical shapes and structures such as wires and antennas[6-8]. The aim of this research is to study, modify, and control the properties of the oxide skin and utilize the properties for producing soft, flexible and functional microfluidic devices that can change shape in response to stimuli.

Conventional electronic devices are generally fabricated from rigid materials (e.g., copper, aluminum, and gold) but these devices experience irreversible damage under deformation

due to cracking and yielding. There is great interest in making electronics flexible (and stretchable) because of the new applications that emerge[16]. Examples include conductive textiles[17,18], paper like flexible displays[19,20,21], conducting skin[22], scanners[23], RFID tags[24,25], solar cells[26], non volatile memory[27] and photovoltaics[28]. We note that most electronic devices consist of multiple types of materials, including semiconductors, insulators, and conductors, but our work focuses only on conductors, which are vital in nearly all electronic devices. Typically, flexible electronics are fabricated by making conventional materials thin (e.g., aluminum foil is flexible). However, thin film geometries on flexible substrates cannot be stretched significantly because of induced fracture upon strain[29-31]. Several groups have addressed this problem by using buckled structures (that fold like an accordion) and therefore offer greater flexibility[32-34]. Liquids are highly deformable and therefore are an appealing material for stretchable electronic devices. However, liquids often have low electrical conductivity and high vapor pressure, which restricts the applicability of familiar liquids (e.g., water, brine) in flexible electronic devices. Moreover, most of the liquids can not be micromolded into useful shapes due to surface tension that seeks to minimize the free surface energy. We address these aforementioned challenges by harnessing the rheological properties of EGaIn. EGaIn, despite of its high surface tension (~640 mN/m), is stabilized mechanically in microchannels because of the presences of the surface oxide skin[5]. By rupturing this surface oxide, EGaIn has already been tailored for many microfluidic devices like reconfigurable antennas[6,8], microfluidic electrodes[15], and memory resistors[35].

In general, the oxide interface that forms on metals (e.g., EGaIn composite) is important for nanotechnology, surface science, semiconductors, microfluidics and microelectronics[36-42]. Chemical and electronic interactions are the two most common research thrusts for metal/oxide interfaces[43]. The adhesion strength[43,44] and mechanical stability or rupture[45-47] behavior are less characterized, yet particularly important for liquid metal systems. In this study, the mechanical stability and rupture behavior of the oxide layer will be characterized by exploiting rheological and electrochemical principles.

## 1.3 Background

### i) Liquid metals

There are four known elements that are liquid at (or near room temperature): mercury, gallium, cesium, and rubidium. Rubidium is radioactive and cesium is explosive. Mercury is the most common room temperature liquid metal but its high surface energy, its toxicity, and its density makes it unfavorable for microfluidic applications[5,48]. Gallium is a compelling liquid metal because it has a low viscosity (like mercury)[49], but forms a surface oxide[1] that stabilizes it mechanically in microchannels[5]. Gallium melts at 30 °C[50] and is therefore technically a solid at room temperature (although it is known to super cool readily)[51,52].

Other low melting metals (e.g., indium, zinc and tin) form alloys that depress the melting point of gallium below room temperature[50]. We focus on eutectic gallium indium because it is the simplest of these alloys (i.e., it is binary) and much is known about its properties. It

melts at 15.7 °C[5] and has an extremely low vapor pressure at ambient temperature[49,53]. The surface of EGaIn oxidizes readily to form a passivating layer[1] (i.e., it does not grow thicker with time) which we call a 'skin'. The skin consists of oxides of gallium[5], which is the same as that which forms on pure gallium. Thus, most experimental conclusions from EGaIn (regarding its skin) are most likely to be applicable for other alloys of gallium too, like, GaInSn (Galistan). Furthermore, literature surveys on gallium and its surface oxide are typically relevant to EGaIn since gallium dominates the important interfacial properties. The following section enlists some of the key properties of gallium, which is followed by the background on surface oxide.

**ii) Properties of Gallium**

Pure gallium is an odorless soft, grey white metal having a rhombic face centered crystal lattice[49,54] ( a = 4.517, b = 4.511, and c = 7.645 ); in liquid form it closely resembles mercury[49]. One of the key features of gallium and its alloys is they remain liquid over a wide range of temperatures[49,51,55,56]. Of all the elements, gallium has the largest range between its melting point (30 °C) and its boiling point (~2200 °C).

Gallium has several interesting properties that occur during freezing. It can be supercooled to a temperature below its melting point up to $-40^0$C[51] (i.e., 70 C below its freezing point). Supercooling of liquid metal is affected by the presence of the surface oxide that provides the seed crystal to initiate homogeneous or heterogeneous nucleation[57-59]. The density of gallium

in the liquid state (6.095 g/cm$^3$) is larger than the solid state (5.904 g/cm$^3$), resulting in 3.2% increase in volume when it solidifies[49,60] Electrical conductivity of liquid gallium is higher than solid gallium because of the increase in co-ordination number in the molten state[49,60]. This property suggests that liquid is more metallic than the solid gallium. Electrical resistance and thermal expansion of solid gallium are different along the three crystallographic planes[49,60].

**iii) Surface oxide on liquid metal**

The surface of gallium and EGaIn oxidize rapidly in air to form an oxidized surface which is mostly oxides of gallium (amorphous). Among all the polymorphs[61,62] of gallium oxide, β-$Ga_2O_3$[63-65] is chemically[66] and thermally stable[62,67]. It is a wide band gap[68-70] transparent n-type semiconductor with amorphous structure. It has been widely used as a gas sensor[68,71-73], luminescent phosphor[74], transparent oxide[66], catalyst[72,75,76], insulator[64,77] for gallium based semiconductors, nanowires and nano ribbons, in laser lithography, solar cells, and optoelectronic devices[78-83].

The rate at which the oxide film forms on gallium and EGaIn is not well understood and is one of our research focuses. However, it is known that the oxide skin forms quickly in air (less than a second) and is passivating (i.e., does not grow thicker with time)[1]. This type of formation generally follows logarithmic decay rule and the structure is not thermodynamically stable because the surface gets compressed due to fast formation[84,85].

The surface oxide on EGaIn is an elastic solid that acts as a membrane to support the metal until it yields[5]. It is strong enough to support the material below its critical limit but it ruptures in response to external stimuli that creates stress more than its critical value (~0.5-0.6 N/m surface yield stress)[5]. EGaIn can be induced to flow in microchannels if the applied stress is higher than the yield stress of the surface oxide skin.

## 1.4. Approach

The oxide skin governs the electrical, mechanical, and chemical properties of the surface of the metal. The ability to flow and stabilize the liquid metal on demand for shaping it to useful responsive structures (e.g., RF-antenna) relies on the rupture of the oxide skin and its reformation. The liquid metal can be induced to flow into microchannels if the applied pressure exceeds the critical pressure (i.e., pressure necessary to yield the skin). The critical pressure scales inversely with the smallest dimension of the microfluidic channel and directly with the critical yield stress of the skin. Therefore, it is possible to tune the critical pressure by changing the geometry of the microfluidic channels.

Based on these principles we have produced a shape shifting antenna and microstrip fluidic filter, which will be discussed in **Chapter 2** and **Chapter 3**. The goal of this work is to control the way in which metal changes shape, and therefore function, in microchannels.

The mechanical properties of EGaIn as a composite can be tuned by modifying the skin, which would also likely modify the chemical and electrical properties of the interface. Fundamental studies of the mechanical properties of the surface of EGaIn will be carried out by rheological measurements. In a stress controlled rheometer, EGaIn will be sandwiched in between a parallel plate of the rheometer and surrounded by aqueous, acidic and organic environments. We will measure the modified mechanical property (i.e., yield stress) of EGaIn interface in these environments. The results suggest that the environment changes the nature of the skin.

In order to detect the real time oxidation and rupture of the oxide layer, we will utilize an amperometric technique. Electrochemical measurements will help establish a "current-voltage-droplet shape" signature or calibration curve that will allow us to characterize the rupture process. We are also interested in ultimately integrating the rheology and electrochemistry in a novel manner so as to elucidate the oxide skin rupture and resulting changes in mechanical properties in real time. When the oxide skin ruptures, the skin weakens and the fresh metal surface gets exposed and is prone to reoxidize.

By integrating the rheology and electrochemistry, we seek to harness these two mechanisms (i.e., rupture and oxidation) simultaneously. As a first step towards this integrated analysis, we will describe an amperometric analysis to elucidate rupture of the oxide skin in aqueous environments.

## 1.5 Overview of the thesis

This thesis combines fundamental studies with applications utilizing EGaIn. Chapters 2 and Chapter 3 illustrate the importance of the skin to control the shape of EGaIn to produce electronic devices (an antenna and a microstrip filter) that change shape, and thus function, in a controlled response to pressure. **Chapter 2** is adapted from a publication in *Applied Physics Letters (Issue 1, Volume 99, 2011).* **Chapter 3** is in preparation for submission to *IEEE Microwave Theory and Techniques.*

**Chapters 4** and **5** explain fundamental studies on the mechanical and electrochemical properties of the metal, respectively. We aim to control and modify the surface of the liquid metal under different stress controlled environments and monitor the change in yield properties of the surface in real time. **Chapter 5** describes an electrochemical analysis to detect the surface rupture or failure of the metal.

## References

[1] M. J. Regan, H. Tostmann, P. S. Pershan, O. M. Magnussen, E. DiMasi, B. M. Ocko, and M. Deutsch, Physical Review B **55** (16), 10786 (1997).

[2] S. J. French, D. J.Saunders, and G. W.Ingle, The Journal of Physical Chemistry **42** (2), 265 (1937).

[3] D. Zrnic and D. S. Swatikd, Journal of less common metals **18**, 67 (1969).

[4] U. König and W. Keck, Journal of the Less Common Metals **90** (2), 299 (1983).

[5] Michael D. Dickey, Ryan C. Chiechi, Ryan J. Larsen, Emily A. Weiss, David A. Weitz, and George M. Whitesides, Advanced Functional Materials **18** (7), 1097 (2008).

[6] J. H. So, J. Thelen, A. Qusba, G. J. Hayes, G. Lazzi, and M. D. Dickey, Advanced Functional Materials **19** (22), 3632 (2009).

[7] M. Kubo, X. F. Li, C. Kim, M. Hashimoto, B. J. Wiley, D. Ham, and G. M. Whitesides, Advanced Materials **22** (25), 2749 (2010).

[8] M. R. Khan, G. J. Hayes, J. H. So, G. Lazzi, and M. D. Dickey, Applied Physics Letters **99** (1), 013501 (2011).

[9] S. Cheng, Z. G. Wu, P. Hallbjorner, K. Hjort, and A. Rydberg, Ieee Transactions on Antennas and Propagation **57** (12), 3765 (2009).

[10] S. Cheng, A. Rydberg, K. Hjort, and Z. G. Wu, Applied Physics Letters **94** (14), 144103 (2009).

[11] H. J. Kim, T. Maleki, P. Wei, and B. Ziaie, Journal of Microelectromechanical Systems **18** (1), 138 (2009).

[12] H. J. Kim, C. Son, and B. Ziaie, Applied Physics Letters **92** (1), 011904 (2008).

[13] R. C. Chiechi, E. A. Weiss, M. D. Dickey, and G. M. Whitesides, Angewandte Chemie-International Edition **47** (1), 142 (2008).

[14] M. M. Thuo, W. F. Reus, C. A. Nijhuis, J. R. Barber, C. Kim, M. D. Schulz, and G. M. Whitesides, Journal of the American Chemical Society **133** (9), 2962 (2011).

[15] J. H. So and M. D. Dickey, Lab on a Chip **11** (5), 905 (2011).

[16] S. R. Forrest, Nature **428** (6986), 911 (2004).

[17] E. R. Post, M. Orth, P. R. Russo, and N. Gershenfeld, Ibm Systems Journal **39** (3-4), 840 (2000).

[18] R. V. Gregory, W. C. Kimbrell, and H. H. Kuhn, Synthetic Metals **28** (1-2), C823 (1989).

[19] Y. Chen, J. Au, P. Kazlas, A. Ritenour, H. Gates, and M. McCreary, Nature **423** (6936), 136 (2003).

[20] J. A. Rogers, Z. Bao, K. Baldwin, A. Dodabalapur, B. Crone, V. R. Raju, V. Kuck, H. Katz, K. Amundson, J. Ewing, and P. Drzaic, Proceedings of the National Academy of Sciences of the United States of America **98** (9), 4835 (2001).

[21] G. H. Gelinck, H. E. A. Huitema, E. Van Veenendaal, E. Cantatore, L. Schrijnemakers, Jbph Van der Putten, T. C. T. Geuns, M. Beenhakkers, J. B. Giesbers, B. H. Huisman, E. J. Meijer, E. M. Benito, F. J. Touwslager, A. W. Marsman, B. J. E. Van Rens, and D. M. De Leeuw, Nature Materials **3** (2), 106 (2004).

[22] T. Someya, Y. Kato, T. Sekitani, S. Iba, Y. Noguchi, Y. Murase, H. Kawaguchi, and T. Sakurai, Proceedings of the National Academy of Sciences of the United States of America **102** (35), 12321 (2005).

[23] T. Someya, Y. Kato, S. Iba, Y. Noguchi, T. Sekitani, H. Kawaguchi, and T. Sakurai, Ieee Transactions on Electron Devices **52** (11), 2502 (2005).

[24] P. F. Baude, D. A. Ender, M. A. Haase, T. W. Kelley, D. V. Muyres, and S. D. Theiss, Applied Physics Letters **82** (22), 3964 (2003).

[25] E. Cantatore, T. C. T. Geuns, G. H. Gelinck, E. van Veenendaal, A. F. A. Gruijthuijsen, L. Schrijnemakers, S. Drews, and D. M. de Leeuw, Ieee Journal of Solid-State Circuits **42** (1), 84 (2007).

[26] A. C. Mayer, S. R. Scully, B. E. Hardin, M. W. Rowell, and M. D. McGehee, Materials Today **10** (11), 28 (2007).

[27] J. Y. Ouyang, C. W. Chu, C. R. Szmanda, L. P. Ma, and Y. Yang, Nature Materials **3** (12), 918 (2004).

[28] G. Yu, J. Gao, J. C. Hummelen, F. Wudl, and A. J. Heeger, Science **270** (5243), 1789 (1995).

[29] T. Saito, T. Furuta, J. H. Hwang, S. Kuramoto, K. Nishino, N. Suzuki, R. Chen, A. Yamada, K. Ito, Y. Seno, T. Nonaka, H. Ikehata, N. Nagasako, C. Iwamoto, Y. Ikuhara, and T. Sakuma, Science **300** (5618), 464 (2003).

[30] S. P. Lacour, J. Jones, S. Wagner, T. Li, and Z. G. Suo, Proceedings of the Ieee **93** (8), 1459 (2005).

[31] T. Tamai, Ieee Transactions on Components Hybrids and Manufacturing Technology **5** (1), 56 (1982).

[32] D. S. Gray, J. Tien, and C. S. Chen, Advanced Materials **16** (6), 477 (2004).

[33] D. S. Gray, J. Tien, and C. S. Chen, Advanced Materials **16** (5), 393 (2004).

[34] R. H. Reuss, B. R. Chalamala, A. Moussessian, M. G. Kane, A. Kumar, D. C. Zhang, J. A. Rogers, M. Hatalis, D. Temple, G. Moddel, B. J. Eliasson, M. J. Estes, J. Kunze, E. S. Handy, E. S. Harmon, D. B. Salzman, J. M. Woodall, M. A. Alam, J. Y. Murthy, S. C. Jacobsen, M. Olivier, D. Markus, P. M. Campbell, and E. Snow, Proceedings of the Ieee **93** (7), 1239 (2005).

[35] Hyung-Jun Koo, Ju-Hee So, Michael D. Dickey, and Orlin D. Velev, Advanced Materials **23** (31), 3559 (2011).

[36] Ulrike Diebold, Surface Science Reports **48** (5-8), 53 (2003).

[37] G. A. Somorjai, F. Tao, and J. Y. Park, Topics in Catalysis **47** (1-2), 1 (2008).

[38] G. D. Wilk, R. M. Wallace, and J. M. Anthony, Journal of Applied Physics **89** (10), 5243 (2001).

[39] E. Budianu, M. Purica, F. Iacomi, C. Baban, P. Prepelita, and E. Manea, Thin Solid Films **516** (7), 1629 (2008).

[40] T. Minami, Semiconductor Science and Technology **20** (4), S35 (2005).

[41] C. Joachim, J. K. Gimzewski, and A. Aviram, Nature **408** (6812), 541 (2000).

[42] J. Mannhart and D. G. Schlom, Science **327** (5973), 1607 (2010).

[43] Qiang Fu and Thomm Wagner, Surface Science Reports **62** (11), 431 (2007).

[44] F. Ernst, Materials Science & Engineering R-Reports **14** (3), 97 (1995).

[45] J. C. Grosskreutz and M. B. McNeil, Journal of Applied Physics **40** (1), 355 (1969).

[46] A. Needleman, Journal of the Mechanics and Physics of Solids **24** (6), 339 (1976).

[47] A. Needleman, International Journal of Solids and Structures **13** (5), 409 (1977).

[48] J. E. Chandler, H. H. Messer, and G. Ellender, Journal of Dental Research **73** (9), 1554 (1994).

[49] I. A. Sheka, I. S. Chaus, and T. T. Mityureva, *The Chemistry of Gallium*. (Elsevier Publishing Company, NewYork, 1966).

[50] T. J. Anderson and I. Ansara, Journal of Phase Equilibria **12** (1), 64 (1991).

[51] Taisiya I. Popova, Irina A. Bagotskaya, and Edward D. Moorhead, *Encyclopedia of Electrochemistry of the Elements*. (Marcel Dekker, Inc., New York, 1978).

[52] L. J. Briggs, Journal of Chemical Physics **26** (4), 784 (1957).

[53] K. A. Narh, V. P. Dwivedi, J. M. Grow, A. Stana, and W. Y. Shih, Journal of Materials Science **33** (2), 329 (1998).

[54] V. Y. Prokhorenko, V. V. Roshchupkin, M. A. Pokrasin, S. V. Prokhorenko, and V. V. Kotov, High Temperature **38** (6), 954 (2000).

[55] J. Jach and F. Sebba, Trans. Faraday Soc **50**, 226 (1953).

[56] V. P. Maiboroda, Thin Solid Films **195** (1-2), 357 (1991).

[57] E. F. Borra, G. Tremblay, Y. Huot, and J. Gauvin, Publications of the Astronomical Society of the Pacific **109** (733), 319 (1997).

[58] J. H. Perepezko, Materials Science and Engineering **178** (1-2), 105 (1994).

[59] John H. Perepezko, Materials Science and Engineering **65**, 125 (1984).

[60] A. G. Lyapin, E. L. Gromnitskaya, O. F. Yagafarov, O. V. Stal'gorova, and V. V. Brazhkin, Journal of Experimental and Theoretical Physics **107** (5), 818 (2008).

[61] R. Roy, V. G. Hill, and E. F. Osborn, Journal of American Chemical Society **74** (3), 719 (1952).

[62] M. Zinkevich and F. Aldinger, Journal of the American Ceramic Society **87** (4), 683 (2004).

[63] N. Ueda, H. Hosono, R. Waseda, and H. Kawazoe, Applied Physics Letters **71** (7), 933 (1997).

[64] T. Harwig and J. Schoonman, Journal of Solid State Chemistry **23** (1-2), 205 (1978).

[65] M. R. Lorenz, J. F. Woods, and R. J. Gambino, Journal of Physics and Chemistry of Solids **28** (3), 403 (1967).

[66] M. Fleischer and H. Meixner, Journal of Applied Physics **74** (1), 300 (1993).

[67] F. K. Shan, G. X. Liu, W. J. Lee, G. H. Lee, I. S. Kim, and B. C. Shin, Journal of Applied Physics **98** (2) (2005).

[68] H.H. Tippins, Physical Review **140** (1A), A316 (1965).

[69] D. J. Fu and T. W. Kang, Japanese Journal of Applied Physics Part 2-Letters **41** (12B), L1437 (2002).

[70] Hajnal Zoltán, Miró József, Kiss Gábor, Réti Ferenc, Deák Péter, C. Herndon Roy, and J. Michael Kuperberg, Journal of Applied Physics **86** (7), 3792 (1999).

[71] M. Ogita, K. Higo, Y. Nakanishi, and Y. Hatanaka, Applied Surface Science **175**, 721 (2001).

[72] D. Kohl, T. Ochs, W. Geyer, M. Fleischer, and H. Meixner, Sensors and Actuators B-Chemical **59** (2-3), 140 (1999).

[73] M. Fleischer, S. Kornely, T. Weh, J. Frank, and H. Meixner, Sensors and Actuators B-Chemical **69** (1-2), 205 (2000).

[74] Orita Masahiro, Ohta Hiromichi, Hirano Masahiro, and Hosono Hideo, Journal of Applied Physics **77** (25), 4166 (2000).

[75] A. L. Petre, A. Auroux, P. Gelin, M. Caldararu, and N. I. Ionescu, Thermochimica Acta **379** (1-2), 177 (2001).

[76] K. Shimizu, A. Satsuma, and T. Hattori, Applied Catalysis B-Environmental **16** (4), 319 (1998).

[77] L. Nagarajan, R. A. De Souza, D. Samuelis, I. Valov, A. Borger, J. Janek, K. D. Becker, P. C. Schmidt, and M. Martin, Nature Materials **7** (5), 391 (2008).

[78] M. Rebien, W. Henrion, M. Hong, J. P. Mannaerts, and M. Fleischer, Applied Physics Letters **81** (2), 250 (2002).

[79] K. L. Chopra, S. Major, and D. K. Pandya, Thin Solid Films **102** (1), 1 (1983).

[80] W. S. Shi, Y. F. Zheng, N. Wang, C. S. Lee, and S. T. Lee, Advanced Materials **13** (8), 591 (2001).

[81] S. Sharma and M. K. Sunkara, Journal of the American Chemical Society **124** (41), 12288 (2002).

[82] Z. R. Dai, Z. W. Pan, and Z. L. Wang, Journal of Physical Chemistry B **106** (5), 902 (2002).

[83] H. Z. Zhang, Y. C. Kong, Y. Z. Wang, X. Du, Z. G. Bai, J. J. Wang, D. P. Yu, Y. Ding, Q. L. Hang, and S. Q. Feng, Solid State Communications **109** (11), 677 (1999).

[84] N. Cabrera and N. F. Mott, Reports on Progress in Physics **12** (1), 163 (1949).

[85] Albert T. Fromhold Jr, Regina G. Fromhold, C.H. Bamford, F. H. Tipper, and R. G. Compton, in *Comprehensive Chemical Kinetics* (Elsevier, 1984), Vol. 21, pp. 1.

# CHAPTER 2: A FREQUENCY SHIFTING LIQUID METAL ANTENNA WITH PRESSURE RESPONSIVENESS

## 2.1 Introduction

This chapter describes antennas fabricated from a liquid metal alloy that can change their electrical length and thus, frequency in response to pressure. Most antennas have a singular, static shape that defines their performance. Reconfigurable antennas, in contrast, can alter their functional behavior (e.g., frequency, bandwidth, or polarization)[1,2] by changing the shape of conductive elements of the antenna[3]. This approach typically involves mechanical or electrical switches (e.g., MEMS, diodes, RF MEMS capacitors)[3-14] that selectively connect and disconnect conductive segments to the antenna. Stretchable antennas composed of liquid metal encased in elastomer can change their physical shape, and therefore resonant frequency, in response to strain[15-17]. Here, we present an antenna architecture that can change its shape in a simple manner by inducing the conductive antenna elements to flow (and merge) in response to external stimuli without using any external switches. The challenge with this approach is to control the way the liquid metal changes its shape so that the response is predictable and rapid. We address this challenge by harnessing the rheological properties of a low viscosity[18], conductive[19] liquid metal alloy (eutectic gallium indium[20], EGaIn, 75% gallium and 25% indium) that is stabilized mechanically within microchannels despite its large surface tension due to the presence of a solid oxide skin[18] that forms spontaneously on

its surface and does not grow thicker with time (i.e., it is passivating[21]). Previous rheological measurements confirm the elastic nature of the skin and establish that it yields beyond a critical stress[22]. We designed a microfluidic channel in such a way that an initially short dipole antenna (~25 mm long) would merge with adjacent segments of metal to create an elongated dipole (~51 mm long) when exposed to a pressure above the critical value required to yield the skin. The merging process changes the shape, and therefore resonant frequency (in three distinct states), in a predictable manner. Because the process of merging is irreversible in its current form, the resonant frequency of the antenna represents a spectral memory state that records the pressure to which it is exposed and offers a simple approach for sensing and recording stimuli (e.g., pressure) wirelessly. This chapter demonstrates and models this frequency-shifting fluidic antenna and elucidates the mechanism by which it changes its shape.

## 2.2 Results

Figure 1 describes the concept of frequency shifting antennas formed by injecting liquid metal into microfluidic channels composed of polydimethylsiloxane (PDMS)[23-25] . The antenna geometry consists of a single row of four collinear segments (each 1 mm wide, 12.6 mm long, 50 μm thick) placed end-to-end. Initially, the two innermost segments comprise the dipole. Two rows of posts (each row consists of 50 μm diameter posts with a 100 μm center-to-center spacing) separate the two innermost segments from the two outermost segments

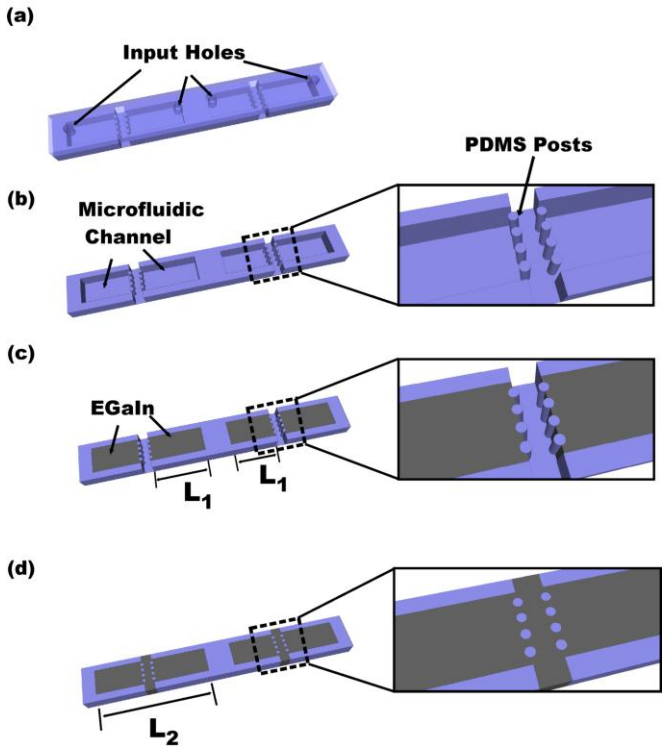


**Figure 1.** A depiction of an antenna that reconfigures its shape in response to pressure (not to scale). a) Empty microchannels with inlet holes (not shown in remaining depictions) b) Rows of posts separate the two outermost segments of the antenna from the two innermost segments. c) Injecting liquid metal into the microfluidic channels produces four antenna segments. Initially, the two innermost liquid segments of length $L_1$ define the dipole antenna. The metal will not flow through the posts until the applied pressure exceeds the critical pressure required to yield the skin that mechanically stabilizes the liquid. d) The four sections of metal merge into two longer sections (each of length, $L_2$), which lowers the resonant frequency.

[Figure 1(b)]. During the fabrication process[26], the metal is injected by hand through the inlet holes (an outlet vent allows air to escape the channel during filling), fills the channels readily, and is stabilized mechanically at the posts by a thin oxide skin [Figure 1(c)]. It does not flow between the posts (the posts acts as Laplace barriers[27]) as long as the critical pressure is not exceeded (the critical pressure depends on the geometry of the posts and is approximately 7 psi for the present geometry)[18]. Pressures that exceed the critical pressure

force the metal to flow between the posts and thereby merge the outermost segments with the inner segments [Figure 1(d)] to increase the physical and electrical length of the dipole.

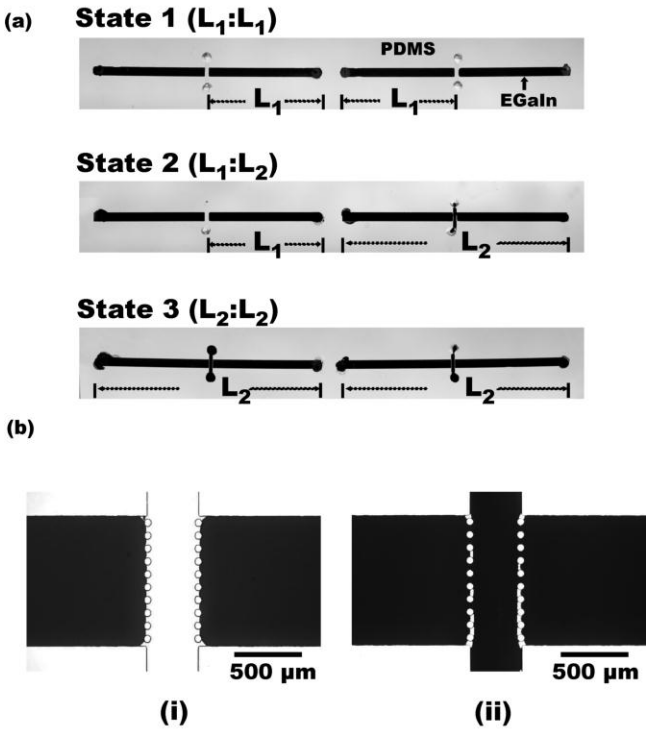


**Figure 2**: Photographs of a shape reconfigurable antenna in three different states. Length $L_1$ is 12.6 mm. a) State 1 consists of four isolated segments of liquid metal embedded in elastomer. The two innermost segments, $L_1$:$L_1$, define the antenna Applying pressure to the right side of the antenna causes two of the sections to merge such that the dipole assumes a different geometry, State 2 ($L_1$:$L_2$). Merging both outermost segments with the innermost segments forms State 3 ($L_2$:$L_2$) b) Micrographs of the region between the segments of metal. i) A narrow gap defined by two rows of posts initially separates the segments. ii) By applying sufficient pressure at the inlet, the metal flows through the posts and merges into an electrically continuous segment.

Figure 2 shows photographs of the antennas in three different states. The two innermost segments comprise the initial dipole antenna with lengths $L_1$ ("state 1"). Pressure applied to one input hole ruptures the oxide skin to produce "state 2" by increasing the length of one

arm of the dipole ($L_2 > L_1$). Pressure applied to the other input hole produces "state 3" in which the dipole consists of two arms, each of length $L_2$. Figure 2(b) shows micrographs of the gap between the PDMS posts before and after merging the metal.

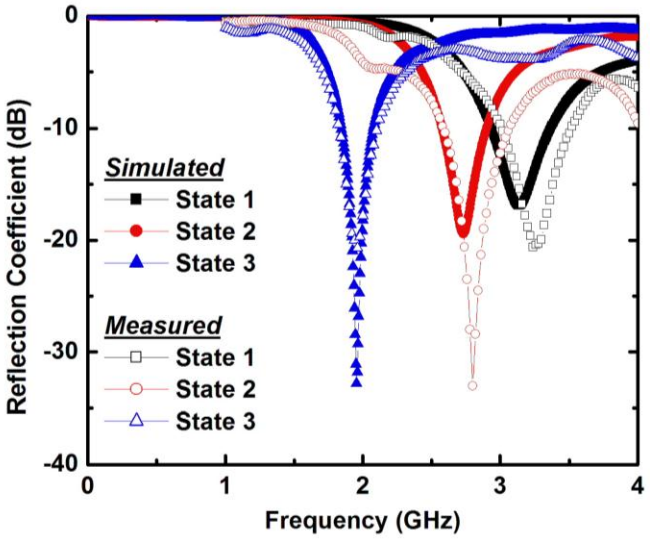


**Figure 3.** Three distinct frequency responses illustrating the frequency shifting nature of the antenna. Measured spectra (open symbols) match well with the simulated spectra (filled symbols). As the arms of the antenna get longer (going from State 1 to 2 to 3), the spectral response of the antenna shifts to a lower resonant frequency.

A coaxial balun featuring two electrical leads connected to the two central arms of the dipole excited the antennas[15]. A network analyzer measured the spectral responses (reflection coefficients) of the antennas and CST-MWS[28] software simulated the spectral response of the antennas. The simulated models of the different lengths of dipoles included the physical and electrical properties of the PDMS substrate ($\varepsilon_r$=2.7 and tan$\delta$ = 0.04) and the liquid metal components[18] ($\sigma = 3.4\times10^4$ *Scm*$^{-1}$); Figure 3 shows that the simulation results and

measurements are in good agreement. As the length of the dipole increases via merging of the segments (from states 1 to 2 to 3), the resonant frequency shifts to a lower value (from 3.6 to 2.6 to 1.9 GHz, respectively, based on the best impedance match), which is consistent with the simulated spectra. The electrically isolated outermost segments in state 1 exhibited minimum electrical coupling to the innermost segments as confirmed by simulation. During the merging process, the metal would often leave small air gaps between some of the posts [e.g., Figure 2(b)]. Based on the model, the trapped air has a negligible effect on the antenna response due to the sufficient electrical connection of the metal between the other posts.

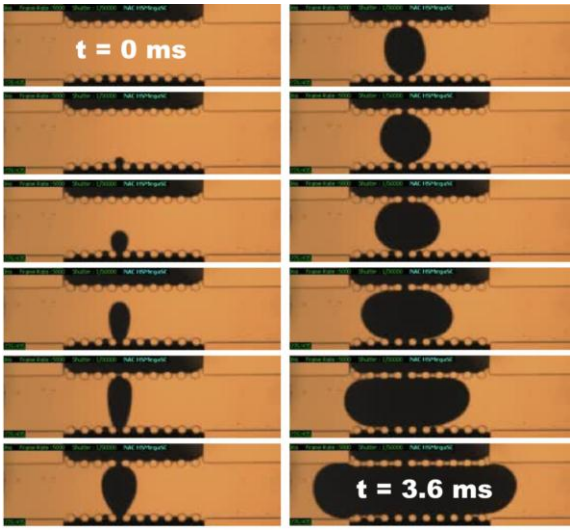


**Figure 4.** Sequential micrographs of the process of merging liquid metal segments. Images are taken from a high speed video camera and each frame represents about 0.3 milliseconds. Pressure applied to the lower segment causes the liquid metal to rupture through two posts and merge with the adjacent metal to form an electrically continuous wire segment and thereby elongate the antenna.

The merging process occurs extremely fast (within a few milliseconds) due to the low viscosity of the liquid metal and the short distance it has to travel. To elucidate the merging process, a video camera with a fast capture rate (5,000 fps) recorded the liquid metal as it ruptures between the posts due to applied pressure. Figure 4 shows 12 chronological frames that capture the merging process over a window of time spanning 3.6 ms. Rupturing occurred at ~8 psi of applied pressure, which is in sufficient agreement with the predicted yield stress (~7 psi) behavior of the skin of the metal for the given geometry[18]. Typically, the liquid metal only ruptures between one set of posts (c.f., Figure 4). This result is consistent with the critical yield stress property of the metal; once the metal ruptures between two posts, the pressure drop at the other metal / air interfaces is no longer sufficient to rupture the skin. The liquid metal merges with the adjacent segment of metal to form an electrically continuous wire before flowing toward the vent holes. Without optimization (and using only our hands to control the pressure applied to the syringe during the initial filling), the segments merged ~75% of the time. In the failures, the wires did not merge due to small air gaps between the two metal interfaces spanning neighboring posts. The yield increased to 100% by either (1) pushing the metal as far as possible through both rows of posts prior to rupturing to increase the chances of merging, or (2) applying pressure to the inlets of both adjacent segments of the metal and thereby forcing the metal to merge.

## 2.3 Conclusion

This chapter demonstrates antennas that change their shape, and therefore frequency, in response to external stimuli (pressure) without utilizing any external switches or electrical connections by inducing a liquid metal to flow and merge into elongated geometries in a predictable manner. This simple approach controls the shape of the active elements of the antenna by exploiting the rheological behavior of the liquid metal that originates from its oxide skin. Modeling of the different states agreed with the experimental results that show shifts of the reflection coefficient response to lower frequencies as the antenna is elongated. Images from a high speed video helped elucidate the mechanism of merging in which metal ruptures between posts when the applied pressure exceeds a critical value.

The ability of the antenna to changes its shape, and therefore function, in response to external stimuli is useful for wireless sensing in which the antenna itself is a sensor. In its current form, the merging process is irreversible and therefore serves as a passive memory element in which hysteretic information is stored in the spectral signature of the antenna. This chapter demonstrates the ability to merge four sections of wires to create three distinct antenna states, but in principle, many different states and geometries are possible. The pressure required to merge the segments could also be tuned by changing the geometry of the posts. In addition to changing the operational frequency (reflection coefficient), the approach could also be used to tune other antenna parameters, such as radiation pattern and polarization. These antennas could be used in wireless sensing or monitoring radio systems,

switches, RFID tags, conformal circuits for health monitoring, or in military applications. An additional advantage of liquid metal antennas is that they adopt the mechanical properties of the encasing material. Antennas encased by elastomer can therefore be bent, twisted and stretched. Here, external pressure altered the shape of the antenna, but it may be possible to use other stimuli (e.g., flexing the antenna) to induce segments of the antenna to merge.

## References


[1] G.H. Huff and J.T. Bernhard, in *Modern Antenna Handbook*, edited by C.A. Balanis (John Wiley and Sons, Inc., Hoboken, NJ, USA, 2008), pp. 369.

[2] J. T. Bernhard, in *Encyclopedia of RF and Microwave Engineering*, edited by K. Chang (Wiley-Interscience, Hoboken, NJ, USA, 2005), pp. 4405.

[3] B. A. Cetiner, N. Biyikli, B. S. Yildirim, and Y. Damgaci, Microwave and Optical Technology Letters **52** (1), 64 (2009).

[4] M. Ali, A. T. M. Sayem, and V. K. Kunda, IEEE Transactions on Vehicular Technology **56** (2), 426 (2007).

[5] A. Mirkamali and P. S. Hall, Microwave and Optical Technology Letters **52** (4), 861 (2010).

[6] G. H. Huff and J. T. Bernhard, IEEE transactions on Antennas and Propagation **54** (2), 464 (2006).

[7] B. A. Cetiner, H. Jafarkhani, J.Y. Qian, H. J. Yoo, A. Grau, and F. D. Flaviis, IEEE communication Magazine **42**, 62 (2004).

[8] E. R. Brown, IEEE transactions on Antennas and Propagation **49** (10), 1357 (2001).

[9] J. L. Freeman, B. J. Lamberty, and G. S. Andrews, Electronics letters **28** (16), 1502 (1992).

[10] C.J. Panagamuwa, A. Chauraya, and J. (Yiannis) C. Vardaxoglou, IEEE transactions on Antennas and Propagation **54** (2), 449 (2006).

[11] D. Peroulis, K. Sarabandi, and L. P. B. Katehi, IEEE transactions on Antennas and Propagation **53** (2), 645 (2005).

[12] D. Piazza and K.R. Dandekar, Electronics letters **42** (8), 446 (2006).

[13] Y. J. Sung, T. U. Jang, and Y.S. Kim, IEEE Microwave and Wireless Components Letters **14** (11), 534 (2004).

[14] N. Kingsley, D.E. Anagnostou, M. Tentzeris, and J. Papapolymerou, Journal of Microelectromechanicalsystems **16** (5), 1185 (2007).

[15] J.H So, J. Thelen, A. Qusba, G. J. Hayes, G. Lazzi, and M. D. Dickey, Advance Functional Materials **19**, 3632 (2009).

[16] S. Cheng, A. Rydberg, K. Hjort *et al.*, Applied Physics Letters **94** (14), 144103 (2009)..

[17] M. Kubo , X. Li , C. Kim , M. Hashimoto , B. J. Wiley , D. Ham , and G. M. Whitesides, Advanced Materials **22** (25), 2749 (2010).

[18] M. D. Dickey, R. C. Chiechi, R. J. Larsen, E. A. Weiss, D. A. Weitz, and G. M. Whitesides, Advance Functional Materials **18**, 1097 (2008).

[19] D. Zrnic and D. S. Swatikd, Journal of less common metals **18**, 67 (1969).

[20] S. J. French, D. J.Saunders, and G. W.Ingle, Journal of Physical Chemistry **42** (2), 265 (1937).

[21] M. J. Regan, H. Tostmann, P. S. Pershan, O. M. Magnussen, E. DiMasi, B. M. Ocko, and M. Deutsch, Physical Review B **55** (16), 10786 (1997).

[22] R. J. Larsen, M. D. Dickey, G. M. Whitesides, and D. A. Weitz, Journal of Rheology **53** (6), 1305 (2009).

[23] J. C. McDonald and G. M.Whitesides, Accounts of Chemical Research **35** (7), 491 (2002).

[24] B.H. Jo, L. M. Van Lerberghe, K. M. Motsegood, and D. J. Beebe, Journal of Microelectromechanicalsystems **9** (1), 76 (2000).

[25] D. C. Duffy, J. C. McDonald, O. J. A. Schueller, and G. M. Whitesides, Analytical Chemistry **70** (23), 4974 (1998).

[26] Y. Xia and G. M. Whitesides, Angew. Chem. Int. Ed. **37**, 550 (1998).

[27] E. Kreit, M. Dhindsa, S. Yang, M. Hagedon, K. Zhou, I. Papautsky, and J. Heikenfeld, Langmuir **26** (23), 18550 (2010).

[28] CST-Computer Simulation Technology Microwave Studio in http://www.cst.com.

# CHAPTER 3: PRESSURE RESPONSIVE MICROSTRIP FLUIDIC FILTER USING A LIQUID METAL ALLOY

## 3.1 Introduction

This chapter describes the fabrication and characterization of a microstrip filter that can change its spectral filtering properties by changing its geometry in a controlled response to pressure. Conventional microstrip filters are fabricated from printed circuit board (PCB) technology [1, 2], a method of etching patterns on stacked sheets of copper and dielectric. These devices are physically static; that is, they have a single geometry that defines their electronic function. Microstrip filters[3] are commonly used in microwave and RF circuits[4-8] and some of the important applications of filters include rejection of interference or noise in wireless or radar systems, modulation or demodulation of signals, and sensing signals [9-15]. Adapting the filtering functions for these applications often requires frequency tuning [15-17]. Using discrete components, the frequency response of a filter can be tuned by MEMS switches[13,17-21], DC contacts / capacitors[22,23], thin film varactors [24] or PIN diodes[25-27]. For distributed element filters[5], like microstrip filters, the length of the stubs[28,29] is one design factor that affects the filtering characteristics. Here, we present a new approach using a liquid metal as the conductive transmission line and stub. The liquid in the stub flows in response to external pressure. The length of the stub changes in a predictable manner due to the presence of posts that act as barriers in the microchannel [30]. The approach takes advantage of the rheological

properties of eutectic gallium indium (EGaIn[31], 75% gallium 75% and 25% indium), which is a low viscosity[32], highly conductive[33] liquid alloy. The alloy only flows when sufficient pressure is applied to rupture the solid, membrane-like oxide skin that forms spontaneously on its surface[32]. We designed microchannels such that the metal would flow, and thereby change shape, in a predictable manner in response to pressure to make dynamic filters with three spectral states. In their current state, these physical changes are not reversible and can be incorporated as inexpensive, passive switches or sensors of pressure. Here, we describe the fabrication of these filters and model and characterize their filtering performance.

## 3.2 Results

Figure 1 shows the geometry of the microstrip filter consisting of a microfluidic channel shaped as a T-junction that is separated from a conductive copper ground plane (c.f. Figure 2) by a thin layer of polydimethylsiloxane (PDMS) [34-36]. The T-junction consists of a main microstrip transmission line (length ~45mm and width ~ 0.9mm) placed perpendicular to a stub line (length ~26mm, width ~ 0.8mm). A row of PDMS posts separate these two lines. Liquid metal fills the transmission line to create a conductive pathway from one side of the transmission line to the other. In the absence of an applied pressure, the metal does not flow into the stub because the rows of posts act as a Laplace barrier[37]. A Laplace barrier is a geometric constriction through which a fluid cannot pass unless a critical pressure is exceeded (this pressure depends inversely on the size of the constriction). The presence of

two additional rows of posts (that span the width of the stub line) allow the metal to flow into three distinct states depending on the applied pressure (the greater the pressure, the longer the stub length). The posts furthest from the transmission line are the most narrowly spaced, which ensures that larger applied pressures correspond to longer stub lengths. When the stub is a quarter of a wavelength long, the stub presents a short circuit (couples with transmission line) to the transmission line and prevents the power from being transmitted through the transmission line at that frequency.

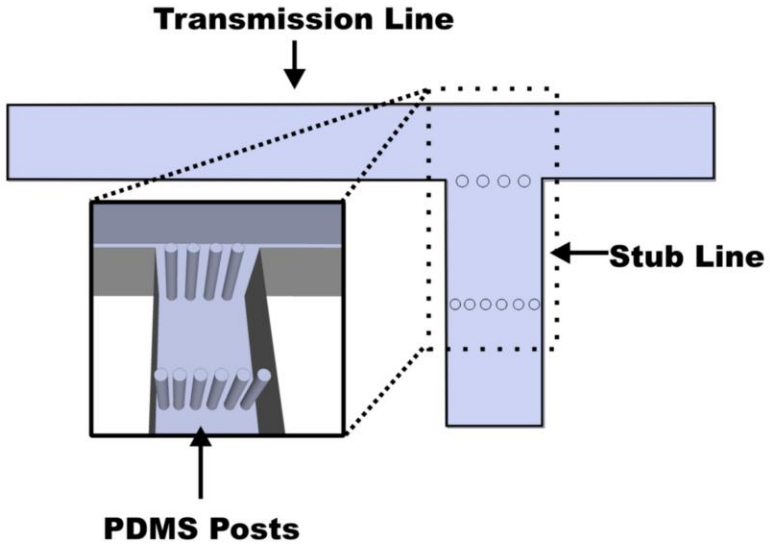


**Figure 1:** A cartoon depiction of the microstrip filter geometry (top view) consisting of a microfluidic channel shaped as a T-junction. This T-junction is used to create shape changing fluidic filter that consists of a transmission line and a stub line. These two lines are placed perpendicular to each other and to be filled with EGaIn to produce different states of the filter. A row of posts (i.e., first row of posts) separates the transmission line from the stub line and an additional row of posts in the stub line allows to create three distinct irreversible states of this filter (c.f. Figure 2).

We define the critical pressure necessary to flow EGaIn through the main transmission line as $P_1$, through the first row of posts (diameter ~ 0.075mm, gap ~0.12mm) as $P_2$, and through the second row of posts (diameter ~0.08mm and gap ~0.06 mm) as $P_3$. We identified post geometries that could be fabricated easily while maintaining large ratios of critical pressures ($P_1$:$P_2$~ 1.5 and $P_3$:$P_2$~ 1.5), estimated using the Young Laplace equation[32]. Injecting the liquid metal through inlet holes into the transmission line by a syringe forms the initial state (state 1) of the filter. The oxide skin on the metal stabilizes it within the transmission line so that it does not flow. Adding co-axial connections to the inlet and outlet of the filled channels and sealing the outlet with more PDMS completes the device. State 2 of the filter arises by applying higher inlet pressure at the inlet hole. This process ruptures the oxide skin that spans the posts and metal flows through the first row of posts to fill readily the stub line up to the next row of posts (i.e., half of the stub line). The second rows of posts are closer together than the first row of posts; thus, the liquid metal ceases to flow and is stabilized again at the second rows of posts. Increasing the pressure further causes the metal to flow through the second set of posts and fill the stub completely with liquid metal. This process produces state 3 of the filter.

Figure 2 shows photographs and micrographs of the filter in three different states. The initial state of the filter is a simple transmission line defined by a microfluidic channel filled with liquid metal (the stub contains no metal). After applying pressure, the metal flows through the first set of posts and stops at the second row of posts to create State 2. At this point, the

stub is only half filled with liquid metal. As we increase the applied pressure (i.e., $>P_2$) "State 3" forms and the stub fills completely.

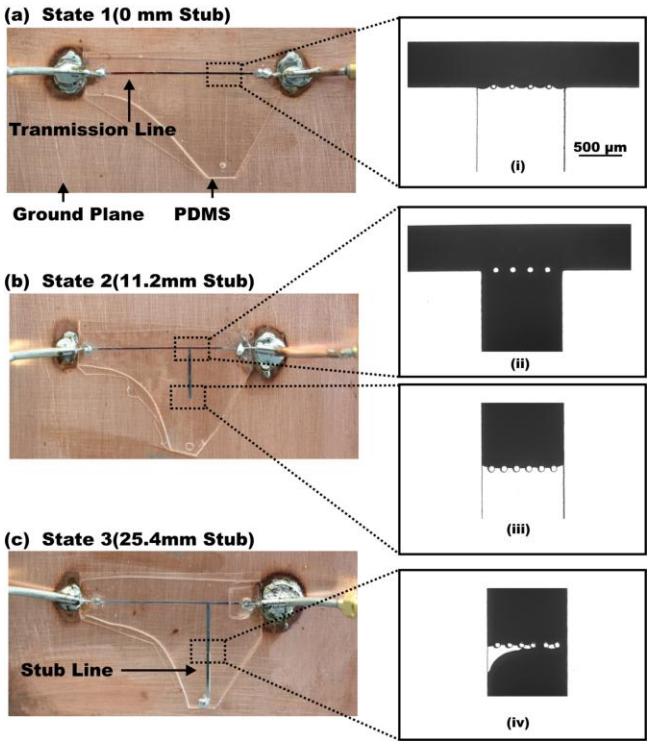


**Figure 2**: Photographs and micrographs of a frequency shifting microstrip filter in three different states. The filter is separated from the copper ground plane by a thin layer (~220 micron thick) of PDMS. a) State 1 consists of a transmission line that is filled with EGaIn and the stub line is empty. The metal is stable due to the oxide skin at the first row of posts as it is shown in (i). b) State 2 of this filter is created by rupturing the oxide and flowing (c.f. inset image (ii)) the metal through the first row of posts by higher applied pressure at one of the ends of the transmission line. Since the dimension (i.e., the gap between the posts) of the posts (i.e., first row and second row) is different, the metal stops at the second row of posts again and it is shown in (iii). c) State 3 of this filter is created by flowing the metal through the second row of posts and micrograph (iv) depicts it

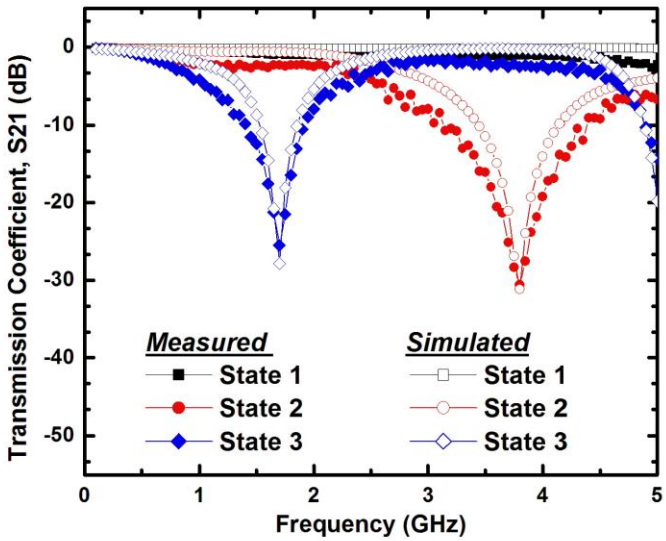


**Figure 3:** Three distinct spectral responses illustrating the frequency shifting nature of the microstrip filter. Measured spectra (closed symbols) agree well with the simulated spectra (open symbols). In state 1 the filter behaves like a transmission line with low transmission loss. As the stub line is filled with the metal, the stub line connects with the transmission line, filters some signal and shifts the frequency to the left. When the stub is completely filled, the filter response is at the lowest frequency.

We measured the spectral response of the filter in all three states using a network analyzer and simulated the spectral response of the filter using CST software (a commercially available electromagnetic simulation tool that uses the finite integral technique in the time domain). The simulated models of the different states of the filter include the physical and electrical properties of the PDMS substrate and the liquid metal components; Figure 3 shows that the simulation results and measurements are in good agreement. In "State 1" the filter consist only of the microstrip element that behaves like a transmission line with low reflection and low transmission loss. As the length of the stub increases (from State 1 to 2 to

3), the filtered frequency shifts to a lower frequency which is consistent with the simulated results.

## 3.3 Conclusion

We fabricated and characterized a tunable microstrip filter consisting of liquid metal that changes its shape in a predictable response to pressure. The filter achieves three frequency signatures that depend on the external stimuli (pressure) without utilizing any electrical switches. Simulation models of the different states agree with the experimental results. Since the stub length is elongated by applied pressure it can be used as a sensor of pressure or as a switchable filter. The simplicity of the fabrication and operation may be useful for low-cost applications where numerous filter elements can be distributed in a grid pattern over a large area to sense changes in pressure. Furthermore, through adjusting the geometry of the posts, the pressure and frequency response ranges can be optimized for the specific application.

## References

[1] M. Carano and J. Fjelstad, in *Electronic Materials and Processes Handbook*, edited by C. Harper (McGraw-Hill, NY, USA, 2004).

[2] R. Lerdwanittip, A. Namsang, and P. Akkaraekthalin, Journal of Semiconductor Technology and Science **11** (1), 65 (2011).

[3] R. Levy and S. B. Cohn, Microwave Theory and Techniques, IEEE Transactions on **32** (9), 1055 (1984).

[4] Y. Fei-Ran, M. Kuang-Ping, Q. Yongxi *et al.*, Microwave Theory and Techniques, IEEE Transactions on **47** (8), 1509 (1999).

[5] G. Bo, T. Ling, and G. Xun, presented at the International Conference on Microwave and Millimeter Wave Technology (ICMMT), Chengdu, 2010.

[6] W. Ching-Kuo, W. Hsien-Shun, and T. Ching-Kuang Cliver, Microwave Theory and Techniques, IEEE Transactions on **50** (8), 1996 (2002).

[7] R. Levy, R. V. Snyder, and G. Matthaei, Microwave Theory and Techniques, IEEE Transactions on **50** (3), 783 (2002).

[8] I. C. Hunter, L. Billonet, B. Jarry *et al.*, Microwave Theory and Techniques, IEEE Transactions on **50** (3), 794 (2002).

[9] K. Jen-Tsai, Y. Tsung-Hsun, and Y. Chun-Cheng, Microwave Theory and Techniques, IEEE Transactions on **53** (4), 1331 (2005).

[10] D. Cañete-Rebenaque, M. Martínez-Mendoza, J. Pascual-García *et al.*, Microwave Theory and Techniques, IEEE Transactions on **59** (2), 242 (2011).

[11] H. Jia-Sheng, M. J. Lancaster, D. Jedamzik *et al.*, Microwave Theory and Techniques, IEEE Transactions on **47** (9), 1656 (1999).

[12] K. Jen-Tsai, C. Sin-Ping, and J. Meshon, Microwave and Wireless Components Letters, IEEE **13** (10), 440 (2003).

[13] I. Gil, M. Morata, R. Fernandez-Gercia *et al.*, presented at the Progress in Electromagnetics Research Symposium Proceedings, Marrakesh, Morocco, 2011 (unpublished).

[14] W. A. Serdijn, M. Broest, J. Mulder *et al.*, Solid-State Circuits, IEEE Journal of **32** (4), 577 (1997).

[15] A. Miller and Hong Jia-Sheng, Microwave and Wireless Components Letters, IEEE **20** (1), 28 (2010).

[16] A. Chauraya, J. Kelly, R. D. Seager *et al.*, presented at the European Microwave Conference 2005 (unpublished).

[17] Y. Liu, A. Borgioli, A. D. Nagra *et al.*, International Journal of Rf and Microwave Computer-Aided Engineering **11** (5), 254 (2001).

[18] K. Entesari and G. M. Rebeiz, Ieee Transactions on Microwave Theory and Techniques **53** (3), 1103 (2005).

[19] P. Blondy, C. Palego, M. Houssini *et al.*, presented at the Asia Pacific Microwave Conference, 2007 (unpublished).

[20] J. Brank, Z. M. J. Yao, M. Eberly *et al.*, International Journal of Rf and Microwave Computer-Aided Engineering **11** (5), 276 (2001).

[21] Q. Y. Song, H. R. Cheng, X. H. Wang *et al.*, Journal of Electromagnetic Waves and Applications **23** (14-15), 2031 (2009).

[22] J. A. Long, C. Z. Li, W. Z. Cui *et al.*, Ieee Microwave and Wireless Components Letters **21** (2), 74 (2011).

[23] A. Pothier, J. C. Orlianges, G. Z. Zheng *et al.*, Ieee Transactions on Microwave Theory and Techniques **53** (1), 354 (2005).

[24] J. Nath, D. Ghosh, J. P. Maria *et al.*, Ieee Transactions on Microwave Theory and Techniques **53** (9), 2707 (2005).

[25] Y. S. Lin, P. Y. Chang, and Y. S. Hsieh, Ieee Microwave and Wireless Components Letters **18** (4), 254 (2008).

[26] C. Lugo and J. Papapolymerou, Iee Proceedings-Microwaves Antennas and Propagation **151** (6), 497 (2004).

[27] W. H. Tu, Ieee Microwave and Wireless Components Letters **20** (5), 259 (2010).

[28] H. Lung-Hwa and C. Kai, Microwave Theory and Techniques, IEEE Transactions on **51** (4), 1241 (2003).

[29] T. Wen-Hua and C. Kai, Microwave and Wireless Components Letters, IEEE **15** (4), 268 (2005).

[30] M.R. Khan, G. J. Hayes, J-H. So *et al.*, Applied Physics Letters **99** (1), 013501 (2011).

[31] S. J. French, D. J.Saunders, and G. W.Ingle, The Journal of Physical Chemistry **42** (2), 265 (1937).

[32] M. D. Dickey, R. C. Chiechi, R. J. Larsen *et al.*, Advanced Functional Materials **18** (7), 1097 (2008).

[33] D. Zrnic and D. S. Swatik, Journal of the Less Common Metals **18** (1), 67 (1969).

[34] J. C. McDonald and G. M.Whitesides, Accounts of Chemical Research **35** (7), 491 (2002).

[35] B.H. Jo, L. M. Van Lerberghe, K. M. Motsegood *et al.*, Journal of Microelectromechanical systems **9** (1), 76 (2000).

[36] D. C. Duffy, J. C. McDonald, O. J. A. Schueller *et al.*, Analytical Chemistry **70** (23), 4974 (1998).

[37] E. Kreit, M. Dhindsa, S. Yang *et al.*, Langmuir **26** (23), 18550 (2010).

# CHAPTER 4: TUNING AND CHARACTERIZING THE INTERFACIAL RHEOLOGICAL PROPERTIES OF A LIQUID METAL ALLOY

## 4.1 Introduction

The goal of this chapter is to study and modify the mechanical properties of a thin oxide skin[1,2] that forms spontaneously on a room temperature liquid metal, eutectic gallium indium (EGaIn)[2,3]. This thin oxide skin allows the liquid metal to be micromolded into stable, non-spherical shapes and structures[4]. The ability to shape this liquid metal into useful structures holds great promise for forming stretchable and reconfigurable electronics[5,6], microelectrodes[7], interconnects[8,9], self assembled monolayers[4,10] and antennas[11,12]. Previous rheological measurements[13] confirm the elastic nature of the skin below a critical yield stress (i.e., the stress that causes the skin to rupture and the metal to flow). The ability to shape (or re-shape) the metal relies on the ability to rupture the skin to allow the metal to flow in a controlled manner. This property is particularly important for applications in which the metal is designed to change shape on demand for stimuli responsive devices[5,6]. In this study, we aim to control and modify the mechanical properties of the skin (i.e., the critical yield stress) so that we can tune the pressure that causes it to rupture and therefore flow. We manipulate and measure the mechanical properties of the oxide skin by exposing the metal to different environments (both stress/strain and chemical environments) using a magnetic bearing

rheometer, AR-G2 (TA instrument). The present work is distinguished from conventional bulk rheology since the most important phenomena happen at the interface of the metal.

Rheology is a branch of science that deals with the flow behavior of liquids as well as the deformation of solids [14-16]. A typical rheological analysis includes a wide range of coupled variables such as force, stress, strain, torque, and deformation[15]. Rheological analysis has been used widely to investigate the properties and behavior of a variety of materials like polymers[17-19], melts[20,21], coatings and dyes[16,22,23]. This analysis is also used to characterize changes in microstructures[24] under applied flow. These analyses, however, rely on the rheological characterization of bulk fluid. In our current study, all the unusual properties arise primarily from the thin solid skin on the liquid metal surface. Here, the bulk liquid is of low viscosity (two times that of water)[25], so the oxide skin dominates the mechanical properties. The present analysis, thus, is more similar to interfacial rheological analysis (i.e., the study of the flow properties of interfaces[26,27]) than to bulk rheology.

Interfacial rheology[27] is utilized for determining the flow properties of suspensions, emulsions, foams, proteins and surfactants[28-39]. Interfacial rheology is typically used to elucidate the behavior of surface active molecules, such as surfactants, and therefore requires very sensitive techniques. In contrast, the liquid metal forms a solid oxide skin on its surface that dominates the mechanical properties of the metal relative to the bulk properties. Moreover, the surface of the metal is reactive such that any exposed metal should oxidize rapidly.

We aim to modify the yield properties[40-44] of the liquid metal under different rheological test conditions (stress / strain) as well as under different chemical environments in a set of small amplitude oscillatory shear experiments. Initially, we compare the properties of EGaIn in air, aqueous, and acidic environments. We show that water and acid both weaken the oxide skin, but it can recover its properties upon drying. We also increase the yield stress of EGaIn by coating spontaneously its surface with a polymer, poly-vinyl-alcohol (PVA). Finally, we apply two key findings from the rheological measurements to tune the critical pressure in microfluidic channels by exposing it to water and PVA solution.

## 4.2 Experimental

We used an AR-G2 rheometer[45] (TA Instruments) with parallel plate geometry for all of the experiments. The bottom plate, which contains a peltier element for temperature control, is stationary and the top plate can rotate with an angular frequency, which is set by the low friction bearing motor of the stress controlled rheometer. The two plates sandwich the sample (in this case, EGaIn), which undergoes shear flow due to the movement of the top plate. A variety of rheological experiments can be conducted in this rheometer[45], but we focus on the small amplitude oscillatory stress sweep since large sweeps[46] are related with the characterization of materials after the yield point. All the measurements use eutectic gallium indium (99.99%, from Sigma-Aldrich). Figure 1 provides a schematic of the rheometer setup.

A custom-made acrylic reservoir provides a vessel into which liquids may be added in intimate contact with the liquid metal. The acrylic reservoir has four inlet and outlet holes in it to facilitate the rheological analysis under different environments.

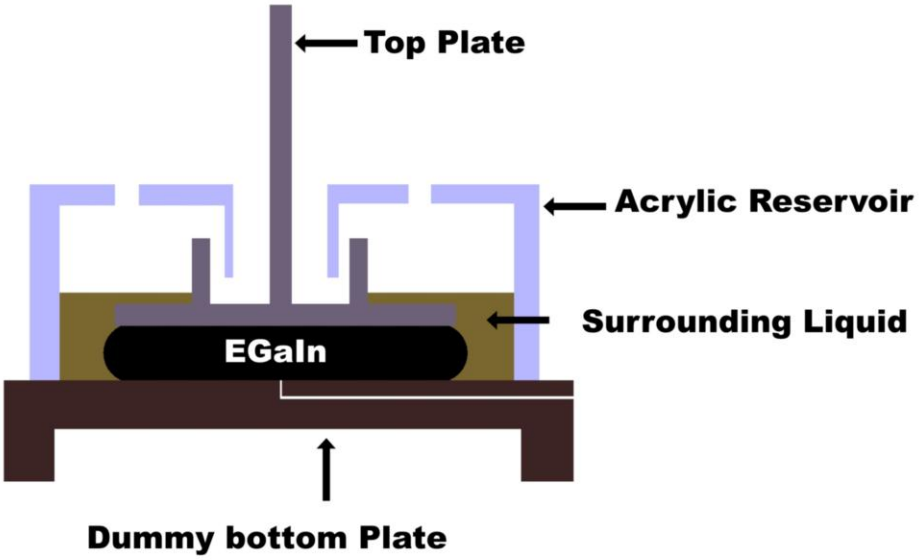


**Figure 1**: A schematic of the experimental setup. EGaIn is sandwiched between a top plate and the stationary bottom plate. To test EGaIn in different environments, an acrylic reservoir fits firmly with the dummy bottom plate. The reservoir is filled with different liquids, which we call "surrounding liquids", to see their effect on the mechanical properties of EGaIn. The top plate rotates with an angular frequency (ω, rad/s) and the bottom plate is kept stationary. All the resistance to top plate movement is generated by the skin on EGaIn and the instrument measures the strain (γ ) while controlling stress (σ, Pa) .

In a typical experiment, we sandwich EGaIn between the top plate and dummy bottom plate. We used a 40mm plastic top plate for most of the experiments. The sandwiched sample volume determines the gap between these two plates, which typically ranges from 1200 μm

to 1600 μm for 0.6 ml to 1 ml samples. To ensure proper sample loading and to avoid sample spreading, the top plate is often lowered with a pre strain rate (± ~0.2/s). We performed all the experiments at room temperature. Before each experiment, we calibrated the instrument (to account for the inertia of the plate and bearing) and zeroed the gap between the top and bottom plates.

## 4.3 Mathematical relationships[14-16]

In a typical small amplitude oscillatory shear experiment, the top plate is rotated with a strain defined as,

$\gamma = \gamma_o \sin \omega t$ ……(1)

The resulting oscillating stress from this strain is given by,

$\sigma = \sigma_0 \sin(\omega t + \delta)$……(2)

Here, $\gamma_0$ and $\sigma_o$ are the strain and stress amplitude, ω is the frequency of oscillation and δ is the phase difference between the strain and stress. The resulting stress has two components and is related with the elastic modulus and viscous modulus as,

Elastic modulus, $G' = (\frac{\sigma_0}{\gamma_0}) \cos \delta$ ……(3)

Viscous modulus, G" = $(\frac{\sigma_0}{\gamma_0}) \sin \delta$ ……(4)

The elastic modulus is in phase with the strain and the viscous modulus is out of phase with the strain. In a period of oscillation, the elastic modulus represents the stored energy in the material while the viscous modulus represents the dissipated energy of the material. For a

perfectly elastic material, strain and stress are in phase (i.e., no phase lag) and the elastic modulus has some finite value with no viscous component. For a purely viscous material, stress is leading by a $90^0$ phase angle and the viscous modulus has a finite value with no elastic component. Most materials share properties of these two extreme materials and are known as viscoelastic.

In a typical rheological experiment (i.e., oscillatory stress sweep in this study) equation (2)-(4) represents the bulk properties of a material. In our study, however, all the rheological properties arise from the surface of liquid metal rather than from bulk metal, which is of low viscosity liquid. The rheometer assumes it is measuring a bulk property and converts torque and strain to bulk stress and modulus. It also assumes that the sample (i.e., the metal) fills completely to the outer diameter of the top plate. Thus, we have to develop relationships to convert bulk stress and modulus for an assumed 40 mm plate to that of a surface stress and modulus using 20 mm of material. All the bulk properties (stress, modulus) of the metal can be converted to surface properties by using the following correlations.

Surface stress, $\sigma_s = K \times C \times \sigma_B$ ……..(5)

Here, K is the plate correction factor, which arises due to differences between the actual diameter of the sample and the diameter of the top plate. Typically, we use a 40 mm (diameter) top plate loaded only up to 20 mm (diameter) due to the expense of the metal.

This constant is equal to $\left[\frac{Plate\ Dia}{Sample\ Dia}\right]^3$. If the sample is loaded perfectly inside the 40 mm plate then this factor is equal to 1. C is a conversion factor that converts bulk properties into surface properties. It is equal to (D/8), in which D (m) is the diameter of the sample. $\sigma_B$ is the bulk stress (Pa) value calculated by the instrument.

The bulk moduli (G' and G") can be converted to surface moduli using the following correlation,

$$G_s' = \left(\frac{R_{plate}}{8}\right) \times G'_B \quad \text{.....(6)}$$

here $G'_s$ is the surface elastic modulus , $G''_B$ is the bulk elastic modulus and $R_{Plate}$ is the radius of the top plate in meters. The viscous modulus (G") can be converted using the same scaling.

We derive the correlation for stress by equating the surface torque of the metal to the bulk torque. We derive the correlations for modulus using,

Stress, $\sigma = G'\gamma + (G''/\omega).\dot{\gamma}^o$ .....(7)

where, $\gamma = Strain = \frac{Radius \times angular\ Displacement}{Gap\ between\ top\ and\ bottom\ Plate}$, and

$\dot{\gamma}^o = Strain\ rate = \frac{angular\ velocity \times Radius}{Gap\ between\ top\ and\ bottom\ Plate}$ .

## 4.4 Results and Discussion

We sought to establish our experimental techniques by first repeating measurements from the literature. We measured the mechanical properties of the metal in air to provide baseline elastic modulus and yield stress values. Figure 2 is a representative plot of the rheological behavior of EGaIn in air acquired using a 40 mm acrylic plate with a 1600 μm plate spacing. We scanned the oscillating stress (bulk) from a low value (~1E-03 Pa) to a high value (25 Pa) at an angular frequency of 1 rad/s without any pre-shear rate in log mode (10 points per decade). All the bulk values are converted to surface values, as shown in Figure 2.

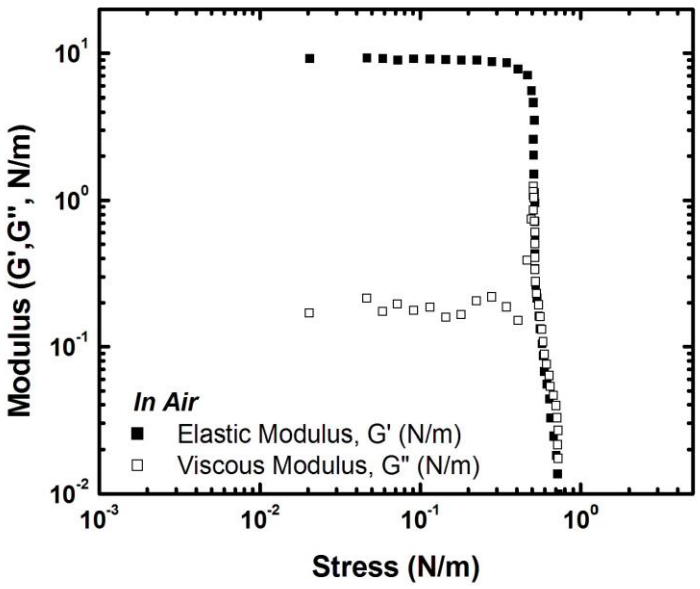


**Figure 2**: Small amplitude oscillatory stress sweep of EGaIn in air. Closed squares are for surface elastic modulus (G',Pa) and open squares are for surface viscous modulus (G",Pa). All the reported values are for surface. The elastic modulus plateaus and dominates relative to the viscous modulus ($\sigma$<0.54 N/m), which is in good agreement with literature. Beyond a critical stress, ($\sigma$ > 0.54 N/m) the liquid metal yields. At the yield point, the viscous modulus crosses over the elastic modulus.

The elastic modulus plateaus ( G'> G", $\sigma \leq \sim 0.54$ N/m) and dominates relative to the viscous modulus. Therefore, the oxide skin behaves as a perfectly elastic material. The yield stress is ~0.54 N/m; any applied stresses less than ~0.54 N/m are not sufficient to yield the skin on the metal. When the applied stress, $\sigma$, exceeds 0.54 N/m, the viscous modulus dominates over the elastic modulus. In this regime, the oxide skin ruptures (elastic modulus exhibits a drastic drop) and the metal flows. The results of this experiment are in good agreement with previous studies[13]. The surface elastic modulus is nearly ~ 10 N/m in the elastic regime and it contains the metal underneath it.

We hypothesized that the surface modulus and yield stress of the oxide skin on EGaIn would not change in the presence of water (relative to that of air) because the viscosity of water is so low. Instead, we found that the modulus and yield stress decreased (relative to that measured in air) in the presence of water. We measured the modulus after filling the acrylic reservoir with deionized water (DI water) while maintaining the same experimental conditions and geometry as that used in air. Since, the metal squirts out between the plates at higher bulk stresses (~30 Pa), we limited the stress between 0.001 to 15 Pa (bulk) without any pre-shearing of the sample. Similar to that measured in air, the elastic modulus plateaus and dominates over the viscous modulus, as shown in Figure 3. However, the elastic modulus decreases by an order of magnitude (~ 1 N/m) relative to that measured in air (~ 10 N/m). The yield stress of the metal also shifts to a lower value in water compared to that in air. In air, it yields at ~0.54 N/m but it drops down to ~ 0.1 N/m in water. This result suggests the

oxide skin is either changing its composition, or getting thinner in water compared to that in air. According to studies of gallium as a dental filling, gallium forms a gelatinous complex of gallium oxide monohydroxides (GaOOH) in water[47], which suggests that the oxide changes its composition in the presence of water. This result is very promising since it suggests that modulus of the skin can be lowered by an order of magnitude and also the yield stress by a factor of 5, simply by exposing it to water. This decrease, thus, will reduce the critical pressure required to flow egain in a prefilled microchannel. (Note: we made the measurements after submerging it for ~10 minutes in water.)

.

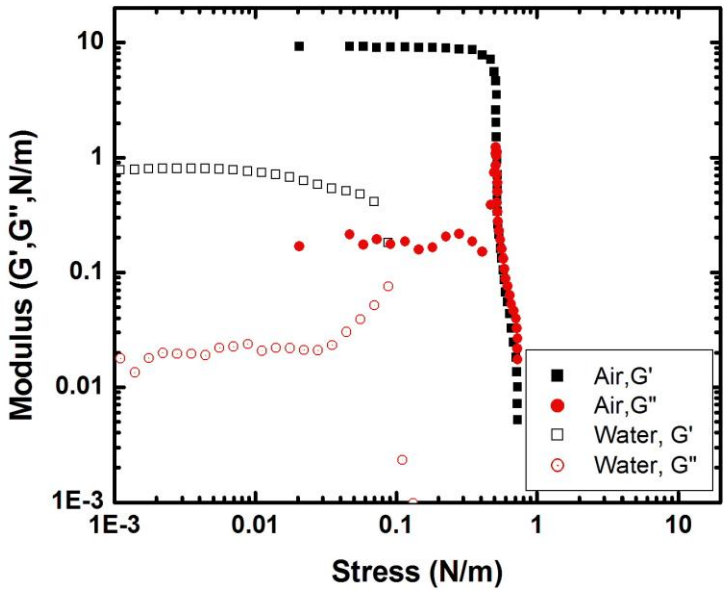


**Figure 3:** Effect of water on the mechanical properties of the oxide skin that forms on EGaIn. During a small amplitude oscillatory stress sweep in water, the elastic modulus gives a plateau near 1 N/m and it yields at 0.1 N/m. The properties of EGaIn in air are included to facilitate comparison. All the closed symbols are for air and open symbols are for water. The elastic modulus is shown by rectangular shape symbols while the viscous modulus is represented by circular symbols. The elastic modulus decreases by an order of magnitude in water. The yield stress is also reduced by approximately a factor of five.

Based on the results from Figure 3, we sought to understand what happens to the mechanical properties of the skin that forms on EGaIn when it returns to a dry state after being submerged in water. We allowed the water to evaporate (waiting more than 96 hours) at room temperature. Figure 4 shows that after drying, EGaIn exhibits a higher elastic modulus (~ 20 N/m) than in air (~ 10 N/m ) or water (~1 N/m). The elastic modulus increases by 2 times that in air and 20 times that in water. The oxidation product of gallium oxide monohydroxides in air may be contributing to this increase in elastic modulus but it is yet to be determined (future work includes a spectroscopic analysis of the surface). The yield stress decreased significantly in water relative to that in air. In contrast, the fully dried sample showed negligible change in yield stress relative to that in air.

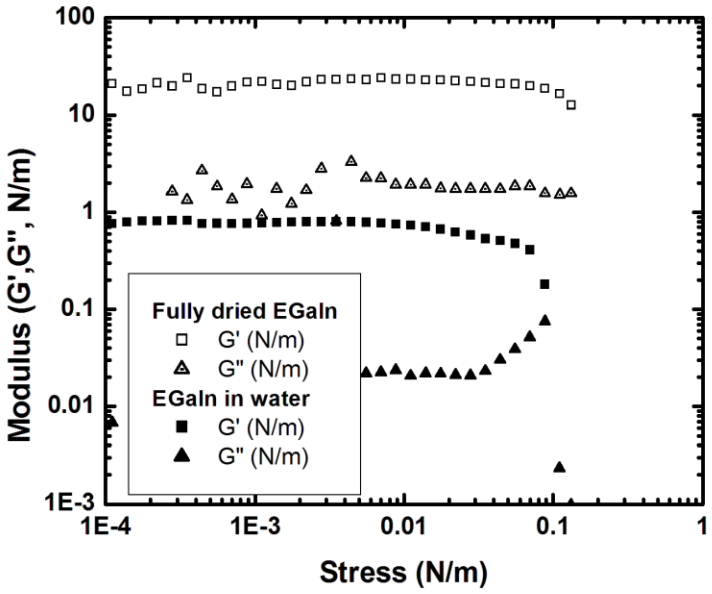


**Figure 4:** Oscillatory stress sweep of EGaIn after the acrylic reservoir is completely dried. The elastic modulus gives a plateau which is larger than the plateau in air. In comparison between a fully dried sample with a sample that is submerged in water, the elastic modulus

increased by 20 times the elastic modulus in water, but the yield stress value does not increase significantly after removal of the water.

The Pourbaix diagram suggests that the oxide skin of EGaIn can be removed by acid (with pH <3)[48]. We commonly use 0.1 M HCl (pH ~ 1) to clean EGaIn from surfaces in the laboratory (e.g., glass slides). As soon as the acid removes the oxide skin, the metals beads up and assumes a spherical shape. We hypothesized that the presence of acid would lower the modulus and eventually remove the skin entirely so that the elastic effects would disappear. We repeated an oscillatory stress sweep in water and then added a few drops of 0.1M hydrochloric acid to water (~pH<1). Figure 5 shows that the yields stress of metal drops upon addition of acid.

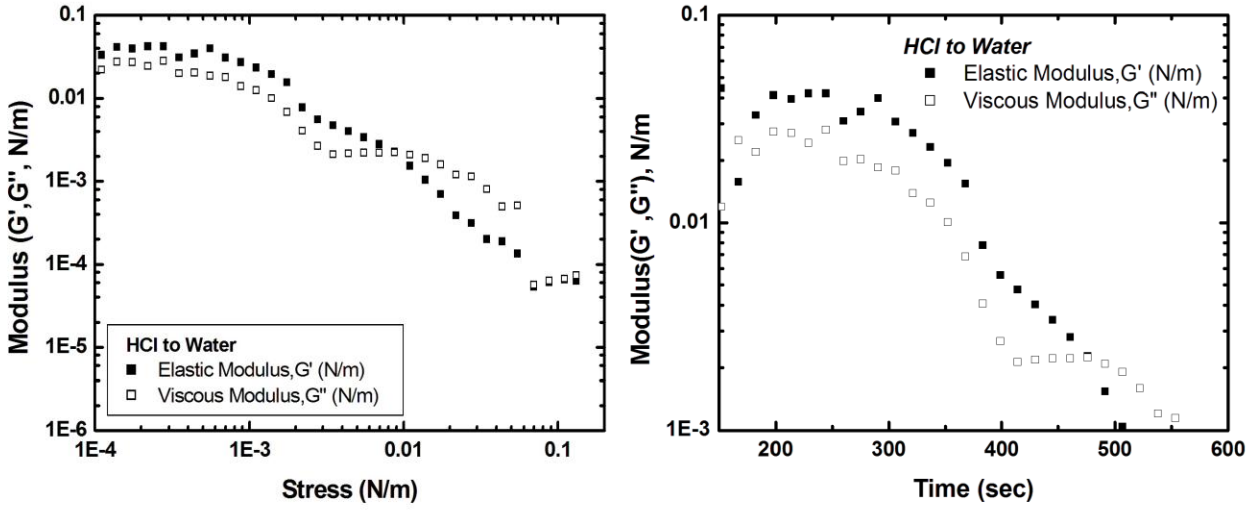


**Figure 5**: Effect of adding a few drops of hydrochloric acid (0.1M) to the water reservoir during an oscillating stress sweep. a) The elastic modulus decreases continuously with surface stress. The yield stress decreases by an order of magnitude in acid relative to that in water. b) The elastic modulus also drops down continuously over time. We suspect that the skin is thinning with the addition of acid as indicated by the continuous decrease in elastic modulus.

The yield stress of the metal drops by an order of magnitude after adding acid. Figure 5 (b) shows the change in elastic modulus over time. The modulus decreases continuously throughout the experiment. This result is expected and proved to be consistent with reported observations of the instability of EGaIn in the presence of acid in microfluidic channels[2]. The elastic modulus also drops drastically by this subsequent acid addition. It is possible that the acid reacts with gallium oxide to produce gallium chloride to reduce the strength of the skin

The overarching goal of this chapter is to tune the yield properties of the metal. The results presented so far indicate the capability of lowering the modulus and yield stress of the surface of the liquid metal by using water and acid. We demonstrated two methods to lower the modulus of the skin, but have yet to demonstrate a method to increase the modulus. We therefore sought to deposit a material from solution onto the skin to increase its thickness and therefore effective modulus. We chose poly-vinyl-alcohol (PVA). It is a commercially available synthetic polymer with water solubility at room temperature[49]. It is a known binder for alumina, ceramics and other materials with surfaces that bare oxides[50-55]. It is known to absorb on a variety of materials including oxides and other polymers[56-58]. Furthermore, we had anecdotal evidence that PVA goes to the interface of EGaIn since it helped stabilize EGaIn droplets from coalescing in water. To investigate the effect of PVA on the effective elastic modulus of EGaIn, we prepared a 1% (wt) solution of PVA in water at room temperature. We used a 20 mm plastic top plate for this experiment and dispensed 0.4 mL of metal in a ~ 800 μm gap between two rheometer plates. We filled the acrylic reservoir with

PVA (1 wt %) to surrounded EGaIn completely by the solution. According to Figure 6, the elastic modulus increased by 4 times relative to the elastic modulus in air. This result is likely due to the deposition of PVA on EGaIn. We measured the kinetics of the deposition of PVA on the liquid metal over time by fixing the oscillatory stress at 5 Pa and collecting a data point every minute over a period of five hours. Figure 7 shows the kinetic study of PVA deposition on EGaIn during five consecutive one hour long time sweeps. It is a cumulative plot which shows the change in modulus over 5 hours.

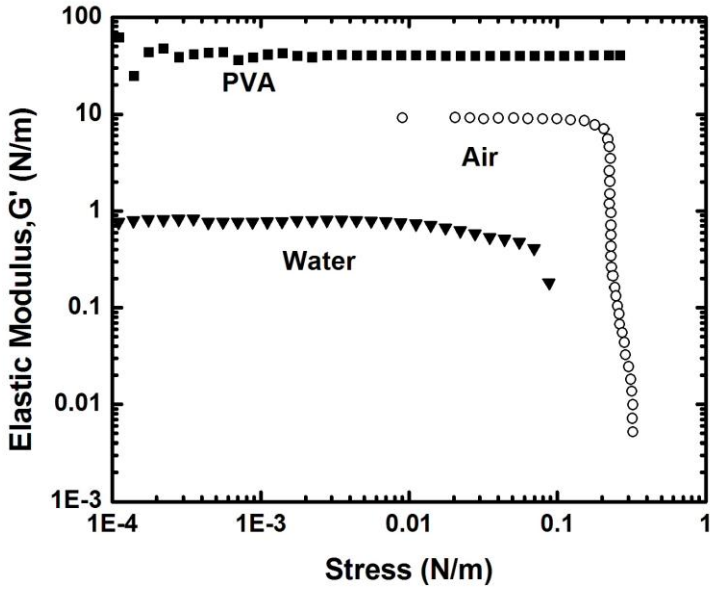


**Figure 6:** Comparison of the elastic modulus of EGaIn in the presence of PVA, air and water. The elastic modulus of the PVA film on EGaIn is ~ 4 times higher than the modulus in air and 20 times higher than the modulus is water. This film did not yield at ~ 0.54 N/m which indirectly indicates the higher yield stress of this film than that in air.

The elastic modulus starts at ~10 N/m and over the next 12~15 min it increases monotonically to ~ 40 N/m. The elastic modulus plateaus around ~ 40 N/m for ~ 1 to 1.25 hr. It shows a plateau followed by an increase in modulus with time as shown in the Figure 7. The oscillating stress– fixed at 5 Pa—was too small to measure any yield point. The elastic modulus increases by two orders of magnitude during this experiment. It is unclear why the modulus levels off before rising again, but we suspect that it could be due to evaporation of water, which could drive PVA out of solution. The elastic modulus does not increase any further other than leveling off at ~ $10^3$ N/m in the last few hours. The plateau of the elastic modulus during this time indicates surface saturation.

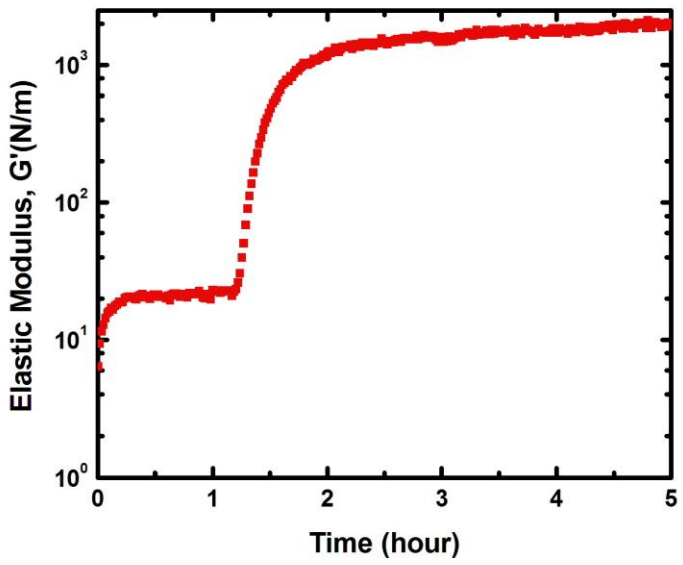


**Figure 7**: The change in modulus on EGaIn as a function of time in the presence of PVA. Over a period of 5 hours, the elastic modulus of this composite is increased by more than two orders of magnitude during 5 successive time sweeps.

Figure 8 shows some microscope images of the PVA coated metal. It is apparent that there is a surface coating on EGaIn. We plan to do a thorough spectroscopic analysis (e.g., XPS and EDS) of the surface of the metal to understand better the surface composition of the films measured in this study, but these images provide visual confirmation of the PVA deposition.

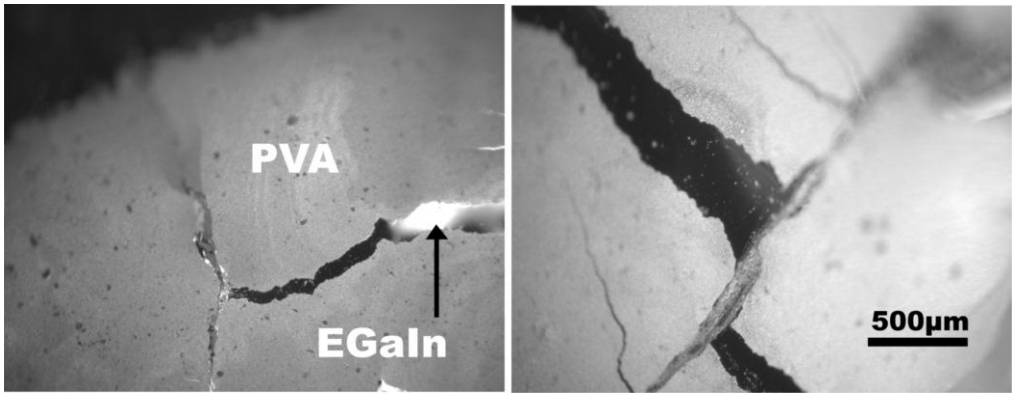


**Figure 8**: Microscope images of the deposited film on EGaIn. The film cracks upon scraping the surface by hand and exposes underlying metal.

## 4.5 Tuning the critical pressure in microfluidic channels

In this section we seek to apply some of the key findings from the rheological analysis to tune critical yield pressure of the metal in microfluidic channels. The ability to tune the yield pressure is important for controlling the flow of metal in microchannels (e.g., Chapter 2). ***Chapter 2*** mentions that the ability to inject liquid metal into microchannels depends on applied critical pressure. The critical pressure depends on the critical dimension of the channel (i.e., the smallest cross-sectional dimension of the channel) and the surface yield stress of the metal. Experiments from rheological characterization of the metal have lead to

two novel approaches to tune the yield properties of the metal using water and PVA. We will apply these two key findings from rheological measurements to see how well they correlate to the response of the metal to pressure in microchannels.

We fabricated a simple, straight microfluidic device by soft lithography and replica molding. Figure 9(a) shows the cartoon depiction of this channel. The length of the channel is 65 mm, width is 1000 μm and the thickness is 100 μm.

We measured the pressure required to fill the channel by EGaIn in the presence of air, so that we can compare it with water or PVA filled channels. In air, 4 to 5 psi (average 4.5 psi) pressure is required to fill the channel completely. We know that the yield stress in air is 0.5 N/m based on rheological measurements. From rheological measurements, we found that the yield stress in water decreased by a factor of 5 relative to that in air. We hypothesized that this decrease in yield stress would also decrease the critical pressure to induce flow of EGaIn in microfluidic channels. To quantify this effect, we first prefilled the channel with water. We used a syringe containing EGaIn and connected it with a pneumatic pressure regulator that can apply and measure pressure. The pressure required to yield the metal in water (2.5 to (3.5 psi with an average of 3 psi) decreased relative to air . The applied pressure, thus, decreased by 33%. This value is lower than that expected based on rheology. This discrepancy could be explained due to the extra pressure required to force the water from the channel.

We repeated this experiment using 1% PVA and found that the pressure required to yield the metal ranged from 3 to 3.5 psi. Rheological analysis showed that the elastic modulus increased by two orders of magnitude in PVA but we have not yet found the yield stress in PVA. The PVA filled channels, did not exhibit significant increase in critical pressure relative to water. We believe observation is due to insufficient time given to deposit the PVA. To harness the effect of PVA more effectively, we prefilled the channel with PVA and injected EGaIn half way into the channel. We waited for 24 hours in hopes that this time would be sufficient to form a PVA film on liquid metal surface. After 24 hours, we found that EGaIn would only flow after exceeding 30 psi. These results are in good agreement with the rheological analysis that mechanical properties change over long time scales. Within 24 hours, PVA deposits as a film on the liquid metal surface which eventually increases the pressure. Some of the water likely evaporated from the channel, which could also increase PVA concentration in the channel.

The rheological analysis showed that the yield properties of the metal return to the native state after being exposed to water and given the opportunity to dry (c.f Figure 4). To test this observation in a microchannel, we filled it with water and injected EGaIn halfway into the channel. From rheological analysis, a fully dried sample shows a larger elastic modulus and negligible change in yield properties after 96 hours. We assumed that 24 hours was sufficient to remove water from the channel but a small amount of water may still be present in the

channel. EGaIn started to flow between 5.5 psi to 7.5 psi (average 6.5 psi). This result also supports our rheological analysis. All these results are summarized in Figure 9.

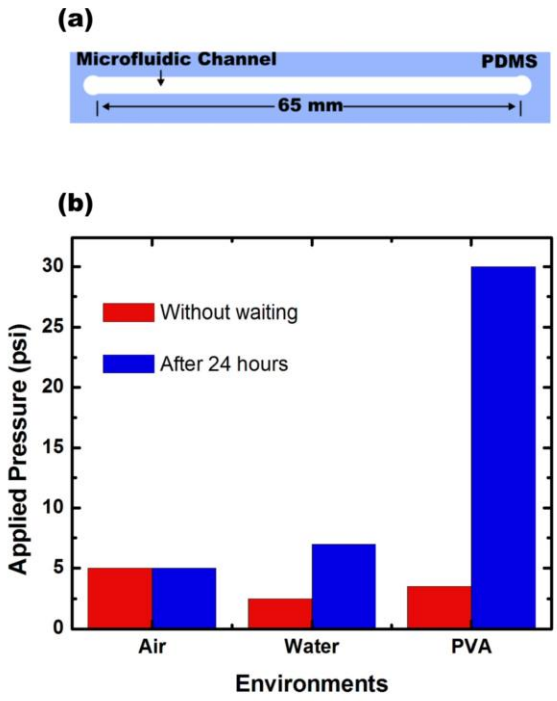


**Figure 9**: Tuning the critical pressure of the liquid metal in microfluidic channels. a) A cartoon depiction of the straight wire which is used for the measurements. We used this straight wire microchannel which is 65 mm long, 1 mm wide and 100 micron thick. b) A bar diagram depicting the required applied pressure to flow EGaIn in the microchannel in presence of air, water and PVA. The pressure required to yield the metal is lower in water than in air, as expected. The PVA changes the pressure after 24 hours of exposure.

In conclusion, all of these results closely match with our rheology results and prove to be in accordance with our hypothesis. The surface of the liquid metal can be modified by water and the deposition of PVA film can actually cause the critical pressure to increase if sufficient time is given for the film formation

## 4.6 Conclusion

The overall goal of this project is to tune the mechanical properties of a surface film on liquid metal and characterize its stability so that it can be tuned on a per application basis. We demonstrated some methodological ways to tune the modulus and yield properties of the of the oxide skin. Tuning the yield properties of the metal is important for defining the stability of the metal in microchannels. In an aqueous environment, the elastic modulus of the metal decreases by an order of magnitude and the yield stress decreases by a factor of two; this result provides a simple approach to reduce the yield stress of the metal. The modulus increases upon drying, but the yield stress returns to the original value measured in air. Poly-vinyl-alcohol deposition on the surface oxide of the liquid metal increased the elastic modulus by several orders of magnitude relative to that in air or water depending on the amount of time it is exposed to the solution. We demonstrate a new in situ method to measure film deposition kinetics by measuring the modulus of thin films deposited from solution. We have also verified these results for microfluidic applications and proved to be in accordance with rheology results. A future goal is to provide spectroscopic analysis of the surface composition of the films produced in these various environments.

## References

[1] M. J. Regan, H. Tostmann, P. S. Pershan *et al.*, Physical Review B **55** (16), 10786 (1997).

[2] M. D. Dickey, R. C. Chiechi, R. J. Larsen *et al.*, Advanced Functional Materials **18** (7), 1097 (2008).

[3] D. Zrnic and D. S. Swatik, Journal of the Less Common Metals **18** (1), 67 (1969).

[4] R. C. Chiechi, E. A. Weiss, M. D. Dickey *et al.*, Angewandte Chemie-International Edition **47** (1), 142 (2008).

[5] J. H. So, J. Thelen, A. Qusba *et al.*, Advanced Functional Materials **19** (22), 3632 (2009).

[6] M.R. Khan, G. J. Hayes, J-H. So *et al.*, Applied Physics Letters **99** (1), 013501 (2011).

[7] J. H. So and M. D. Dickey, Lab on a Chip **11** (5), 905 (2011).

[8] H. J. Kim, C. Son, and B. Ziaie, Applied Physics Letters **92** (1) (2008).

[9] H. J. Kim, T. Maleki, P. Wei *et al.*, Journal of Microelectromechanical Systems **18** (1), 138 (2009).

[10] M. M. Thuo, W. F. Reus, C. A. Nijhuis *et al.*, Journal of the American Chemical Society **133** (9), 2962 (2011).

[11] S. Cheng, Z. G. Wu, P. Hallbjorner *et al.*, Ieee Transactions on Antennas and Propagation **57** (12), 3765 (2009).

[12] M. Kubo, X. F. Li, C. Kim *et al.*, Advanced Materials **22** (25), 2749 (2010).

[13] R. J. Larsen, M. D. Dickey, G. M. Whitesides *et al.*, Journal of Rheology **53** (6), 1305 (2009).

[14] C. W. Macossko, *Rheology Principles, Measurements, and Applications*. (Wiley-VCH, NY, 1994).

[15] Thomas Mezger, *The rheology handbook : for users of rotational and oscillatory rheometers,* 2nd ed. (Vincentz, 2006).

[16] J. F. Steffe, *Rheological methods in food processing engineering*, 2nd ed. (Freeman Press, East lansing, MI, 1996).

[17] S. R. Bhatia, A. Mourchid, and M. Joanicot, Current Opinion in Colloid & Interface Science **6** (5-6), 471 (2001).

[18] L. J. Gerhardt, C. W. Manke, and E. Gulari, Journal of Polymer Science Part B-Polymer Physics **35** (3), 523 (1997).

[19] G. M. Kavanagh and S. B. Ross-Murphy, Progress in Polymer Science **23** (3), 533 (1998).

[20] M. Gahleitner, Progress in Polymer Science **26** (6), 895 (2001).

[21] K. Bernreitner, W. Neissl, and M. Gahleitner, Polymer Testing **11** (2), 89 (1992).

[22] C. Gallegos and J. M. Franco, Current Opinion in Colloid & Interface Science **4** (4), 288 (1999).

[23] E. P. A. Kumbasar and M. Bide, Dyes and Pigments **47** (1-2), 189 (2000).

[24] S. R. Raghavan and S. A. Khan, Journal of Rheology **39** (6), 1311 (1995).

[25] J. N. Koster, Crystal Research and Technology **34** (9), 1129 (1999).

[26] Brian Warburton, Current Opinion in Colloid & Interface Science **1** (4), 481 (1996).

[27] V. V. Krotov, in *Interfacial Rheology*, edited by R. Miller and L. Liggieri (Koninklijke Brill NV, Leiden, Netharlands, 2009), Vol. 1.

[28] C. F. Brooks, G. G. Fuller, C. W. Frank *et al.*, Langmuir **15** (7), 2450 (1999).

[29] Eric Dickinson, Josephine A. Hunt, and Douglas G. Dalgleish, Food Hydrocolloids **4** (5), 403 (1991).

[30] P. Erni, P. Fischer, E. J. Windhab *et al.*, Review of Scientific Instruments **74** (11), 4916 (2003).

[31] J. Kragel, S. R. Derkatch, and R. Miller, Advances in colloid and interface science **144** (1-2), 38 (2008).

[32] R. Miller, R. Wüstneck, J. Krägel *et al.*, Colloids and Surfaces A: Physicochemical and Engineering Aspects **111** (1-2), 75 (1996).

[33] Reinhard Miller, Valentin B. Fainerman, Jürgen Krägel *et al.*, Current Opinion in Colloid & Interface Science **2** (6), 578 (1997).

[34] Brent S. Murray, Current Opinion in Colloid & Interface Science **12** (4-5), 232 (2007).

[35] D. Langevin, Advances in Colloid and Interface Science **88** (1-2), 209 (2000).

[36] C. Alonso, T. Alig, J. Yoon *et al.*, Biophysical Journal **87** (6), 4188 (2004).

[37] J. W. Anseth, A. J. Goffin, G. G. Fuller *et al.*, American Journal of Respiratory Cell and Molecular Biology **33** (2), 161 (2005).

[38] P. J. Carreau, P. A. Lavoie, F. Yziquel *et al.*, in *Rheology Series* (Elsevier, 1999), Vol. Volume 8, pp. 1299.

[39] Jason R. Stokes and William J. Frith, Soft Matter **4** (6), 1133 (2008).

[40] J. R. Stokes and J. H. Telford, Journal of Non-Newtonian Fluid Mechanics **124** (1-3), 137 (2004).

[41] Q. D. Nguyen and D. V. Boger, Annual Review of Fluid Mechanics **24**, 47 (1992).

[42] H. A. Barnes, Journal of Non-Newtonian Fluid Mechanics **81** (1-2), 133 (1999).

[43] D. C. H. Cheng, Rheologica Acta **25** (5), 542 (1986).

[44] H. A. Barnes and K. Walters, Rheologica Acta **24** (4), 323 (1985).

[45] AR-G2 manual, TA instruments, www.tainstruments.com.

[46] K. Hyun, S. H. Kim, K. H. Ahn *et al.*, Journal of Non-Newtonian Fluid Mechanics **107** (1-3), 51 (2002).

[47] N. Horasawa, H. Nakajima, S. Takahashi *et al.*, Dental Materials Journal **16** (2) (1997).

[48] M. Pourbaix, *Atlas of Electrochemical Equilibria in Aqueous Solutions—Gallium*. (National Association of Corrosion Engineers, Houston, Texas, 1974).

[49] G. Rakesh and A. P. Deshpande, Rheologica Acta **49** (10), 1029.

[50] S. Baklouti, T. Chartier, C. Gault *et al.*, Journal of the European Ceramic Society **18** (4), 323 (1998).

[51] D. Santhiya, S. Subramanian, K. A. Natarajan *et al.*, Minerals & Metallurgical Processing **16** (2), 51 (1999).

[52] U. Paik, V. A. Hackley, and H. W. Lee, Journal of the American Ceramic Society **82** (4), 833 (1999).

[53] B. E. Platonov and T. A. Polishchuk, Ukrainskii Khimicheskii Zhurnal **47** (2), 167 (1981).

[54] A. P. Ilin, Y. G. Shirokov, and V. A. Smirnov, Izvestiya Vysshikh Uchebnykh Zavedenii Khimiya I Khimicheskaya Tekhnologiya **25** (4), 452 (1982).

[55] B. E. Platonov, T. A. Polishchuk, and V. M. Kalyuzhny, Dopovidi Akademii Nauk Ukrainskoi Rsr Seriya B-Geologichni Khimichni Ta Biologichni Nauki (11), 41 (1981).

[56] Th F. Tadros and B. Vincent, Journal of Colloid and Interface Science **72** (3), 505 (1979).

[57] Partha Sarathi Roy, Joyeeta Bagchi, and Swapan Kumar Bhattacharya, Transition Metal Chemistry **34** (4), 447 (2009).

[58] Changmei Sun, Rongjun Qu, Chunnuan Ji *et al.*, Journal of Nanoparticle Research **11** (4), 1005 (2009).

# CHAPTER 5: CHARACTERIZING THE RUPTURE AND REFORMATION OF A THIN OXIDE FILM ON EUTECTIC GALLIUM INDIUM USING AMPEROMETRY

## 5.1 Introduction

This chapter describes the development of a new amperometric technique[1] to elucidate the physical failure, rupture, and reformation of a thin oxide film on a room temperature liquid metal alloy, eutectic gallium indium (EGaIn)[2,3]. The oxide skin[4] forms spontaneously and rapidly on the surface of the metal and provides the metal with unusual mechanical properties[3,5]. Above a critical stress, the skin ruptures and allows the otherwise low viscosity liquid to flow[3]. The ability to flow or stabilize the metal on demand is important for shaping it into useful, and in some cases, responsive structures (i.e., those that change shape by flowing in response to some stimuli)[6,7]. When the skin ruptures, the underlying metal gets exposed and is prone to oxidation. We hypothesized that this oxidation event could be detected electrochemically and sought to develop a method to detect these events. These methods could help identify when rupture occurs, quantify how much skin breaks, and determine how fast the skin forms in various environments and geometries. Ultimately, this work will be used to correlate electrochemical signals to changes in the mechanical properties, which will be accomplished by combining rheology and electrochemistry in real time. As a first step toward this integrated analysis, we seek to study the rupture of the oxide

film under controlled mechanical and electrochemical conditions (outside of a rheometer). Amperometric analysis[8-12], one of the most important electro-analytical technique[1,13-15], has been employed widely to detect real-time oxidation or reduction events. Here, we develop a new amperometric technique for measuring the oxidization of metal that takes advantage of the liquid nature of EGaIn. We utilize EGaIn as a working electrode. By expelling the metal out of a syringe at a controlled flow rate, the amount of new surface area created is known. As the EGaIn droplet enlarges, the skin must rupture and oxidation ensues. We seek to measure and understand the amperometric signals arising from this technique.

The electrochemical study of the oxidation of freshly generated metal surfaces is an important phenomenon in erosion/corrosion, environmental cracking, and stress corrosion cracking and corrosion fatigue[16-22]. Electrochemical studies are often carried out to elucidate the kinetics of surface oxidation/reduction on an electrode, predicting the velocity of corrosion cracks and for some other fundamental interests[23-31]. Nearly All metal electrodes (except gold, platinum) are thermodynamically unstable (i.e., the surface oxidizes) at ambient conditions[32,33]. Passive oxide films[33-38] (i.e., those that do not grow thicker with time) on metals, such as the one formed on gallium, are very common and widely studied for aluminum[37,39-45], titanium[16,17,46-48], and steel[19,49]. These films are also important for corrosion protection[22,37]. To study the oxidation process, these passive films are often removed by scrapping, cutting, yielding, rupturing, scratching and shearing[16,17,47,50-57]. As soon as the bare metal is exposed by these mechanical techniques, it repassivates spontaneously, which provides an opportunity to measure electrochemically an oxidation event. The passivation

and repassivation of fresh metal surface is challenging to analyze in these conventional analyses because these techniques are poorly controlled and difficult to implement[58-60].

Our approach for generating fresh metal is novel and relatively simple (relative to conventional brute force methods, such as scraping and cutting). It produces bare metal surface at a known time-averaged rate by pumping the metal with a syringe pump. The drop shape, coupled with the flow rate, gives an accurate estimate of the surface area. We utilize the spontaneous passivation (i.e., oxidation) of EGaIn to establish an electrochemical signature that occurs when a fresh metal surface is exposed (due to rupture) and oxidized (repassivation).

We use a dropping EGaIn electrode as the working electrode, which is similar in geometry to a dropping mercury electrode. The classic electrochemical technique "polarography"[1,61-66,] uses dropping mercury electrode. Expelling Hg from a reservoir creates continuously new electrode surface area. The electrode measures oxidation / reduction reactions from solution and has the appeal of creating continually fresh (i.e., pristine) electrode surfaces. Gallium and EGaIn are not typically used for "dropping electrode" experiments because the surface oxidizes, which makes interpretation of any electrochemical measurement challenging[67,68]. We seek to take this nuisance and use it to understand better the oxidation process itself, rather than using the electrode to perform solution electrochemistry. Because the measurements relate to oxidation, the work is also relevant to corrosion[22,37].

The oxides on gallium and indium are passive under a wide range of conditions. The electrochemical behavior of gallium electrodes has been studied in aqueous, acidic and alkaline environments[69-77]. Electrochemistry of indium has been carried out in chloride, alkaline, acidic and in aqueous environments[78-85] as well. We assume that gallium is the surface active species since it oxidizes much more readily than indium and has proven to be the dominant surface species in air[3]. For this study, we hypothesize that, rupturing and forming the oxide skin will give amperometric signals that can be used as a tool to characterize thin film instabilities (e.g., rupture of the oxide skin) in a number of applications, including microfluidics.

## 5.2 Chronoamperometric analysis[1]

Chronoamperometry[1,8,9,12] (the measurement of current with time) is one of the most widely used electro-analytical techniques to study electrochemical reactions. In chronoamperometry, the working electrode potential is stepped from a rest potential (where no Faradic reaction occurs) to a potential of interest to promote either oxidation or reduction reactions[1]. A potentiostat measures the current passing through the working electrode while holding the potential of interest constant for a certain period of time. It is a direct way of measuring Faradic current (in the case of dilute solutions, this is also called "diffusion current" because reactive species get depleted near the electrode and must diffuse to the electrode). The time dependence of the diffuse Faradic current can be modeled by using Cottrell equation[1].

The Cottrell equation provides a very good estimate of diffusion limited current in a stationary planar electrode. However, the EGaIn electrode is not static; it is similar to the dropping mercury electrode. For dropping mercury electrodes, the Cottrell equation is modified by incorporating the mass flow rate of drops (m), density of drops (ρ) and increase in area of the drop. In a dropping mercury electrode the shape (i.e., radius, r) of the drop increases continuously before falling, so the size of the drop is a function of time (t), density (ρ) and mass flow rate (m) of the drop and is given by,

$$r = \left(\frac{3mt}{4\pi\rho}\right)^{1/3} \qquad (1)$$

Assuming a spherical geometry, the surface area of the drop will be,

$$A = 4\pi\left(\frac{3mt}{4\pi\rho}\right)^{2/3} \qquad (2)$$

Inserting equation 2 into the Cottrell equation gives the Ilkovic equation, which is used commonly in polarography. The Cottrell or Ilkovic equations are for diffusion limited process where the faradic species diffuse from the solution to the electrode. In our studies, the solvent itself (water) is electrochemically active (i.e., gallium reduces it) and therefore it is not dilute. We found that these equations were therefore not appropriate for our analysis and we develop our own analysis later in this study.

Non Faradic current due to electric double layer charging and low level of redox components in the system can also contribute to the overall anodic current during electrochemical analysis, which is given by

$$i_c = \frac{E}{R} e^{\frac{-t}{RC}} \qquad (3)$$

Here, $i_c$ is the charging current, E is the applied potential, R is the solution resistance and C is the double layer capacitance. The charging current decays exponentially with time. If the electrode area, electrode potential or interfacial capacitance varies with time then charging current will come into play.

## 5.3 Experimental

We performed all the experiments using a three electrode systems as shown in Figure 1; liquid metal is the working electrode, platinum wire is the counter electrode and a saturated silver/sliver chloride is the reference electrode (in this chapter, all the applied potentials are vs. Ag/AgCl). All the electrodes are placed as close as possible (~3.5 cm) and the distance between the electrodes is limited by the design of the cell. During an electrochemical process, current flows between the working and counter electrode. The reference electrode helps maintain the potential at the working electrode.

A syringe pump extrudes EGaIn through a polymeric capillary tube to form a nearly spherical drop that hangs from the end of the tube inside the electrochemical vessel. The

shape of this drop increases until its weight can no longer be supported by the interfacial tension of the metal.

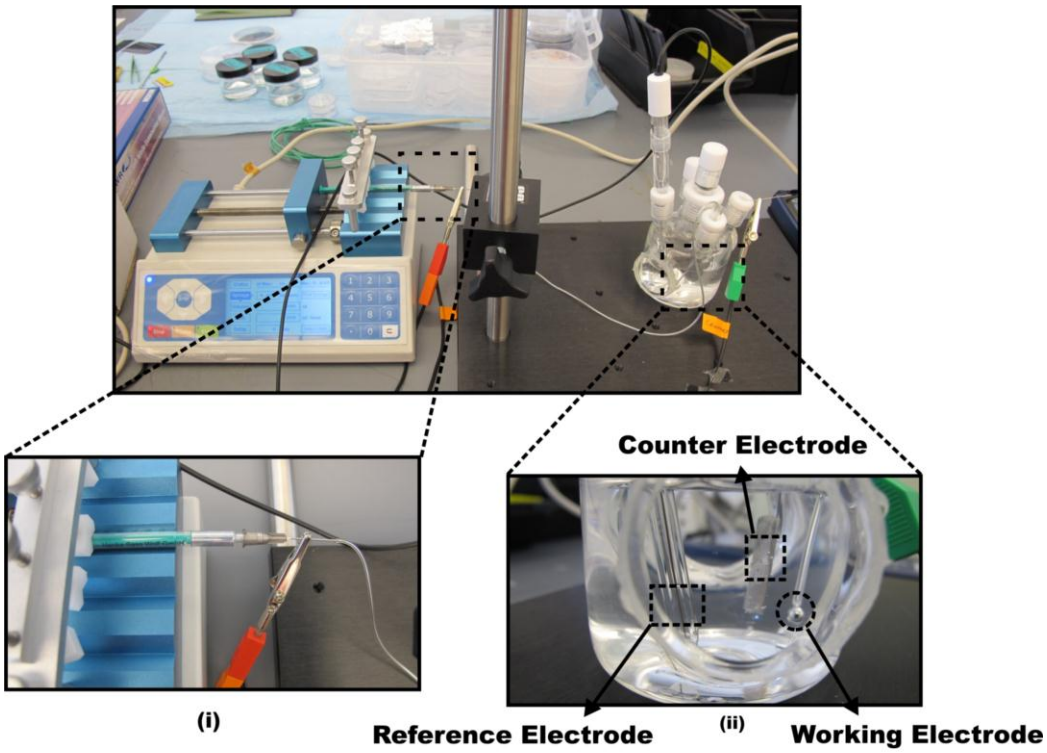


**Figure 1:** Schematic of the electrochemical system used in this study. i) A 1 ml syringe attached to a syringe pump forces metal through a plastic tube into the vessel. An alligator clip connects the potentiostat to the needle of the syringe to complete the connection of the working electrode. ii) Inset image of the cell that includes three electrodes.

The diameter of a representative drop is ~ 2 to 2.8 mm before it falls. The lifetime of a drop varies with the flow rate of extrusion and applied voltage (Reductive potentials prevent the oxide skin from forming and tend to decrease the lifetime of the drop. A secondary consideration is that the surface tension of the metal can change with applied voltage). A

potentiostat measured the current generated as a function of time (Wave Now, Pine Instruments, www.pine.com).

## 5.4 Results

Although it would be easier to interpret oxidation results from pure gallium (rather than EGaIn) since it is a single component system, we chose EGaIn because it is a liquid at room temperature, whereas gallium melts at 30°C. We performed several amperometric experiments with a gallium working electrode. During the experiments, gallium solidifies since the operating temperature is lower than the melting point of gallium. The freezing makes it impossible to pump gallium, which is critical for the experiments. Henceforth, we use EGaIn for all the remaining analysis. We note that gallium has been shown previously to be the surface active species for oxidation since it oxidizes more readily than indium and is in greater concentration than indium in the alloy[3].

Our primary goal was to verify that we could detect the rupture and reformation of the oxide skin using this new amperometric technique. We therefore selected an oxidative potential to ensure the oxide would reform if ruptured. We extruded the metal at 200μl/hr into DI water and kept the voltage constant at 0 V. At 0 V, EGaIn can oxidize spontaneously. Figure 2 shows the results from these measurements. Under these conditions, the lifetime of a drop (i.e., the time between the formation and falling of a drop) is ≈ 200 s. During these experiments, a potentiostat recorded the anodic current every second for 100 minutes.

There is a minimum in current before the drop emerges rapidly from the end of the tube. This lull is apparent in Figure 2b between the two and three minute mark. We observed a 60 s delay between droplets falling and new droplets forming. This delay could be due to the bulging of the flexible tube or trapped air inside the tube. When the new droplet forms, it emerges suddenly from the end of the tube as a droplet with a finite diameter (approximately 0.93 mm diameter as found by calculation), rather than growing slowly. The anodic current peaks at ≈ 70μA when the drop initially emerges from the tube. The sharp increase in current as EGaIn comes out of the tube is likely due to the sudden increase in fresh metal interface, which can lead to oxidation of the surface of the metal (and double layer capacitance)[86]. After the sharp initial peak, the anodic current falls exponentially within ~25 s.

After it suddenly emerges from the tube, the droplet grows slowly until it becomes large enough to fall. As the drop increases in volume with time, we observe a number of small current peaks that each decay rapidly. These peaks include a characteristic decay on the order of ~6 s (Figure 2b). The peaks occur approximately every 1~1.5 s. We hypothesize that these peaks result from the rupture of the oxide skin (and subsequent exposure of the underlying metal), which must occur as the surface area of the drop of EGaIn increases. Finally, when gravitational forces overcome the interfacial tension of the skin, then the drop falls from the end of the tube to the bottom of the cell; this process occurs periodically every ~200 s, which we define as the drop lifetime.

The observation of small peaks suggest that oxide skin is breaking, which causes metal to be exposed and subsequently oxidized. The ability to measure these peaks electrochemically is a successful first step toward the goals of this project and suggests that the rupture of the oxide skin can be detected.

We sought to study the amperometric behavior of the metal under conditions that were more oxidative than 0 V. We repeated the experiments while applying 0.1 V to the working electrode. The anodic current shows similar but more pronounced behavior at 0.1 V to that at 0 V. As expected, the anodic current is larger than those measured at 0 V since there is an additional driving force for oxidation. The lifetime of the drop increases by ~50 to 100 s, which may be attributed to the increased anodization of the skin (that is, a thicker skin should be stronger and thus, support a larger drop). The small decaying peaks form nearly at the same frequency as measured at 0 V and the large current peak decays over 25-30 s.

Because of the similarity of the amperometric behavior of EGaIn at 0 and 0.1 V (Figure 2), we sought to explore more aggressive oxidative conditions; we therefore increased the potential to 1.5 V. Figure 3 shows there is a spike in current when a new droplet first emerges from the tube. This spike decays and then the baseline current grows monotonically.

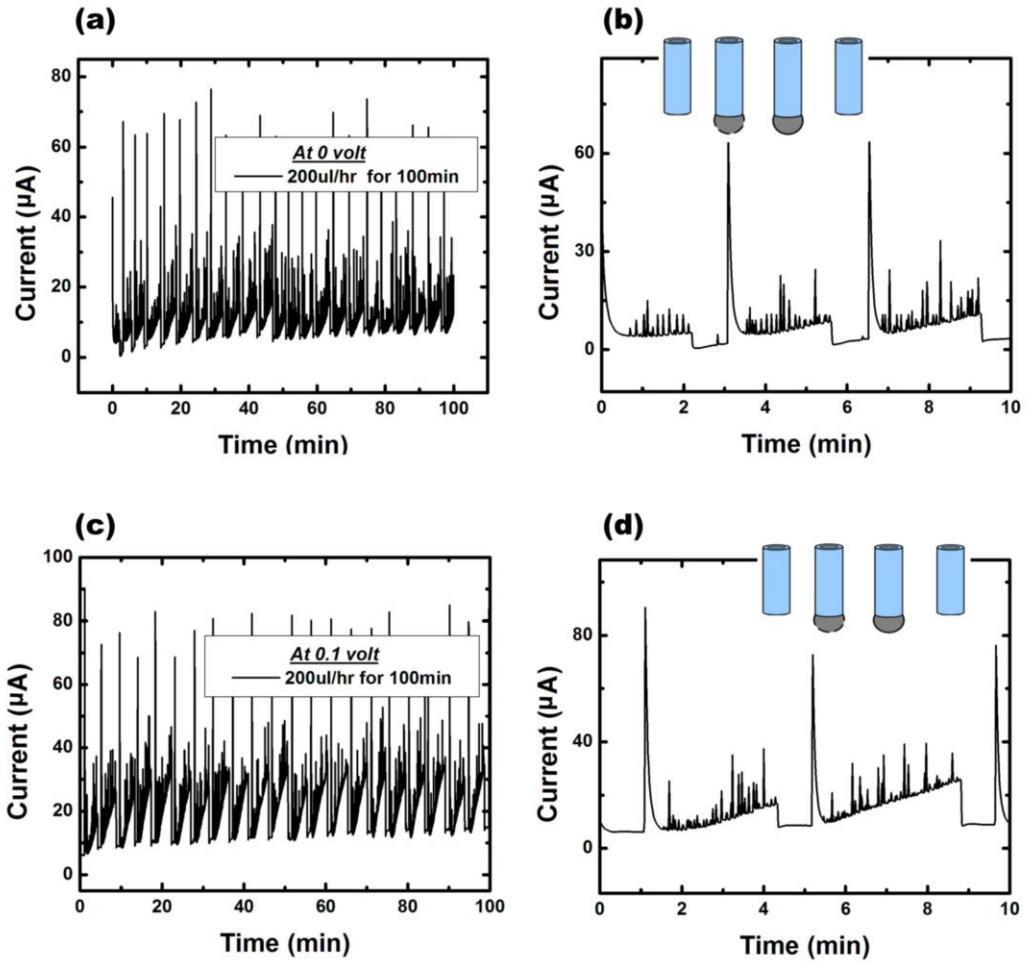


**Figure 2:** Chronoamperometric analysis of EGaIn in DI water at 200 μl/hr. a) Current vs time for EGaIn at 0 V. b) A close up (from 0 to 10 min) of the data from part (a) with a cartoon depiction of the state of the working electrode at the top. As the drop comes out of the tube a sharp positive peak appears that decays quickly. Subsequently, several small peaks appear periodically before the drop falls down. c) Current vs. time relationship of EGaIn at 0.1 V d) Zoom in plot during the first 10 minutes of the study. At 0.1 V the anodic current shows similar behavior, albeit with larger magnitude, as it is at 0 V.

Notably, there are no significant small decaying peaks that occur as the baseline grows.

During this analysis approximately 9 drops come out of the tube (over a 50 minute time span)

and each drop has a lifetime of ~5 min (i.e., longer life than at 0 and 0.1 V). The anodic current decays within 30 s and then it increases with time until the drop falls. The initial spike is likely due to the oxidative current since a significant amount of metal is exposed suddenly.

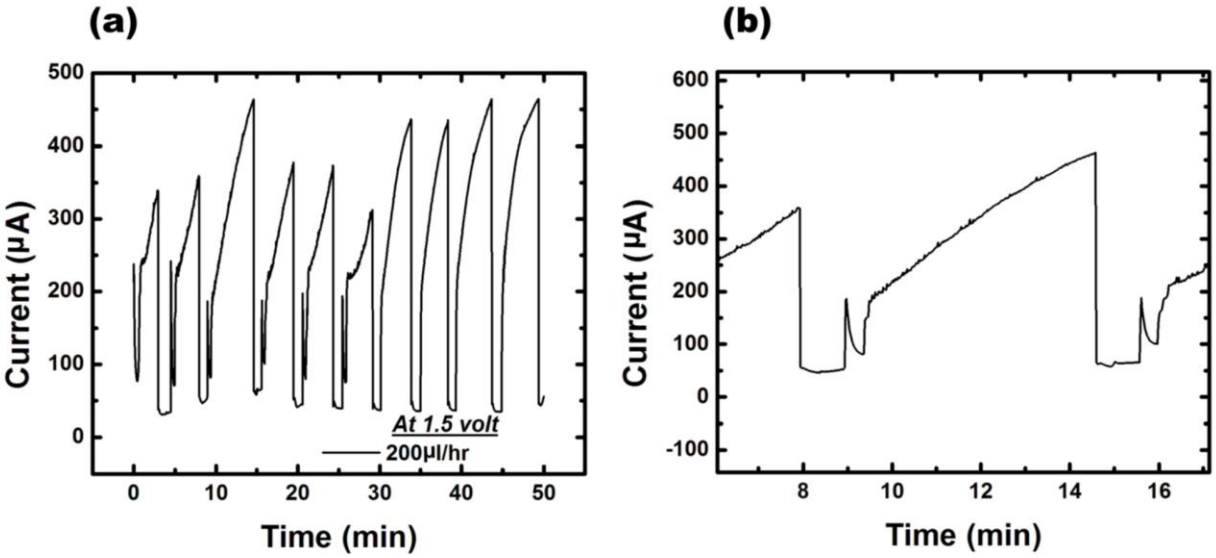


**Figure 3**: The anodic current traces of EGaIn as it is extruded at 200μl/hr into DI water at a fixed potential of 1.5 V (vs. Ag/AgCl). a) Current vs time relationship over the duration of the experiment. b) Zoom in plot during 6-18 min of the analysis. As the drop emerges from the tube it gives an increase in anodic current which is followed by a decay. Then the anodic current increases with time till the drop falls.

After the initial spike, the current increases monotonically and it is nearly six times higher than the current at 0 or 0.1 V. This increase could be due in part to the anodization of the skin (i.e., the skin getting thicker). Note that the initial spikes in current are inexplicably followed by decay in the first six droplets, but not in the following drops. This result suggests there is a transient period at the beginning of the measurements. Interpreting the data is complicated by the tendency of water to electrolyze at the working electrode at this potential. If water is reduced, then it is possible to locally alter the pH near the working electrode

because of $OH^-$ ions. Finally, it is notable that no peaks in current occur as the droplet grows in size, which is in contrast to the behavior observed at 0 and 0.1 V. This result might be explained by the thicker oxide layer, which provides a barrier between fresh metal and the surroundings as the drop grows. As we develop the capability to measure rheology and electrochemistry at the same time, we will have tools available to provide better insight into the subtle behaviors of this system.

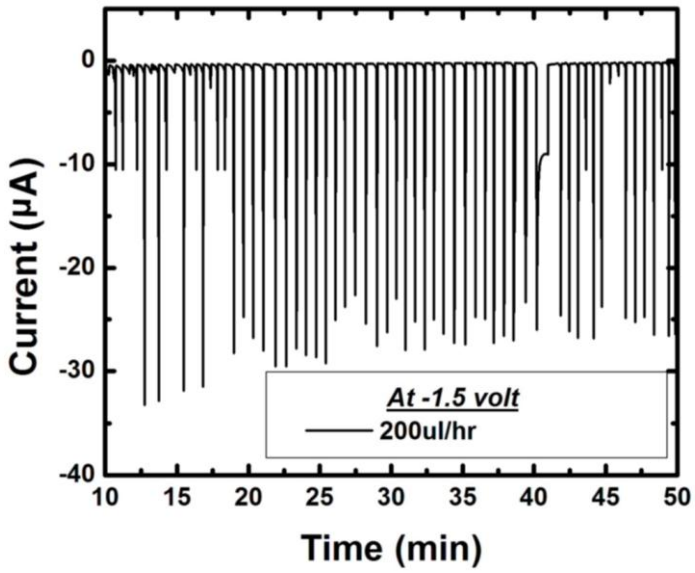


**Figure 4.** Current vs. time of EGaIn at -1.5 V (vs Ag/AgCl) and flow rate of 200μl/hr. This potential is more negative than the standard electrode potential of gallium, so the electrode is cathodically polarized. EGaIn drops fall frequently in this experiment and the current plateaus at ~0 A.

The measurements shown in Figures 2 and 3 suggest the ability to measure oxidation of EGaIn using this new amperometric method. To explore this possibility further, we investigated the amperometric behavior of dropping EGaIn at reductive potentials that prevent any oxidation from occurring (i.e., -1.5 V). According to the Pourbaix[87] (potential-

pH diagram) diagram of gallium, this voltage should be sufficient to keep the metal thermodynamically stable (without passivation) because the standard electrode potential[88] of gallium ($Ga^{+3}/Ga$) is -0.52 V and of indium ($In^{+3}/In$) is -0.34 V. If there is no oxide skin on the surface of the liquid metal, then we expect the small decaying peaks (that we believe are associated with oxidation) to disappear. Figure 4 shows that the current does not exhibit any small decaying peaks, which is consistent with our hypothesis. The baseline current is nearly 0 A with intermittent negative peaks that occur each time a new drop emerges suddenly from the tube (as opposed to the positive peaks we observe under oxidative conditions). New drops formed quite frequently (~7-10 drops in 5 min).

The lifetime of each drop is nearly ~25 s which is nearly an order of magnitude less than that at 0, 0.1, and 1.5 V. As soon as the drop formed, it fell quickly with a significantly shorter lifetime for each drop compared to the lifetime under oxidative potentials for the same flow rate. The short lifetime is likely due to effects of surface tension resulting from the absence of oxide skin; the large surface tension of EGaIn (~640 mN/m)[3] will pinch off any drop as it forms.

The behavior of the current at -0.1 V, despite being negative, shows similar behavior as 0 or 0.1 V. Since the standard electrode potential of the metal is well below -0.1 V, this negative voltage is still sufficient to foster the oxidation of the metal as shown in Figure 5.

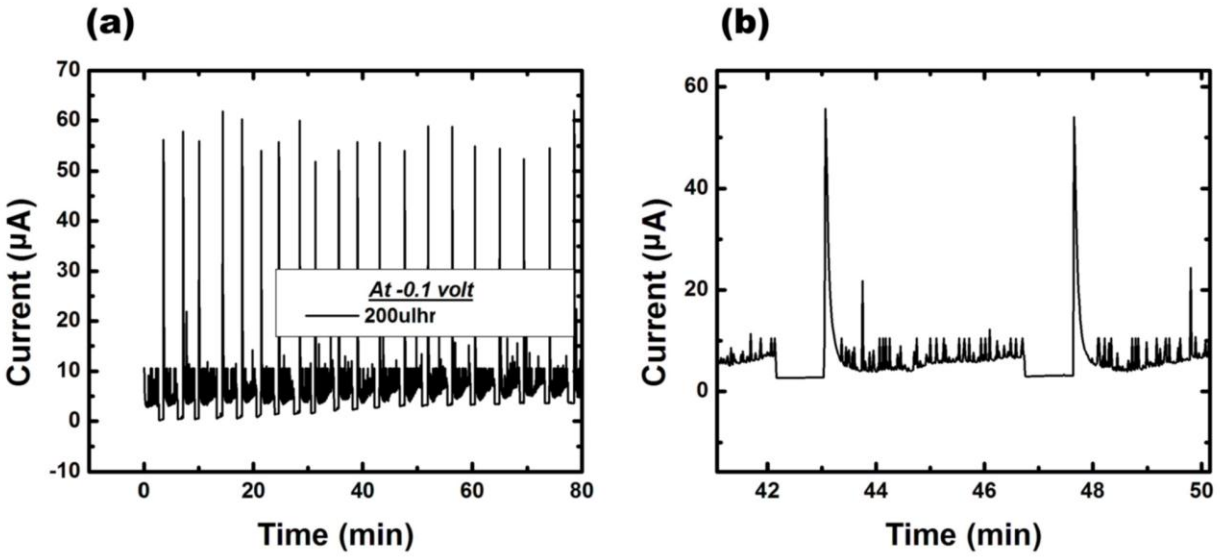


**Figure 5:** Chronoamperometric analysis of EGaIn in DI water at 200μl/hr. a) Current vs time of EGaIn at -0.1 V for 80 minutes. b) A smaller time window of the data plotted in (a). As the drop comes out of the tube a sharp increasing peak occurs and decays quickly. A few small decaying peaks are also observed before the drop falls down. The anodic current exhibits similar trends but is lower in magnitude compared to Figure 2.

All of the data reported to this point have been obtained in DI water. We hypothesized that adding electrolyte could provide additional insight into the measurements. For example, increasing the conductivity of the solution should decrease the decay time associated with any capacitive charging peaks (and thereby provide a way to differentiate capacitive current from faradaic current). We used 0.01M NaCl solution to increase the conductivity of the electrolyte. In a separate experiment, we used 0.1 M HCl solution. Figure 6 presents the current-time traces for both electrolytes. The anodic current shows similar behavior in both of these electrolytes, but shows very different behavior in contrast to 0 V in DI water.

Although the lifetime of each drop is similar to that at 0 V in DI water, there was no lull in current between droplets because the droplet formation is continuous. Also, there were no current spikes. The current increases monotonically as the shape of the droplet increases (suggesting a dependence on electrode area) and suddenly drops down to a lower value as the EGaIn drop falls.

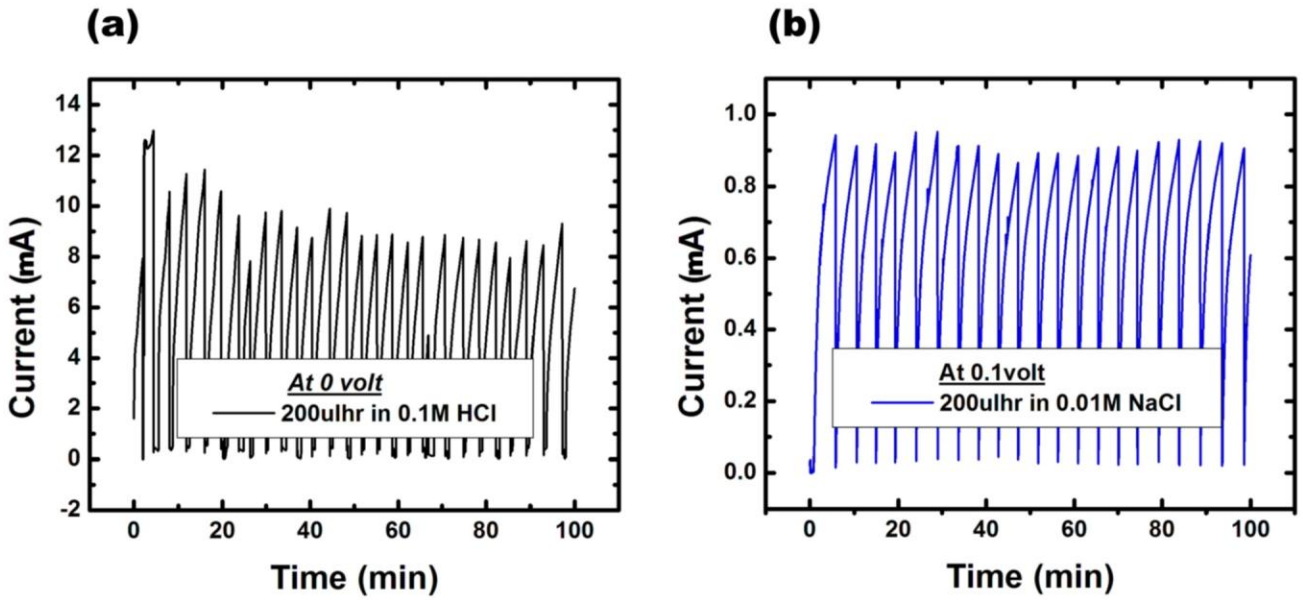


**Figure 6:** a) Chronoamperometric traces in 0.1M HCl acid solution. b) Traces in 0.01M NaCl solution. The flow rate of EGaIn is 200µl/hr. Both of these trends look similar. The anodic current has relatively higher magnitude in HCl solution. Due to higher solution conductivity, the current traces look different from amperometric analysis in DI water.

The magnitude of the current, in both of these solutions, is higher (i.e., 3 orders of magnitude) than that measured in DI water. It is apparent upon comparing Figures 2 and 6 that the presence of electrolyte changed the amperometric behavior of dropping EGaIn relative to DI water. We speculate that the chloride ion is participating in some electrochemical reactions and could explain the increase in current. At larger voltages, ( >1.5

V), we observe the formation of a black shell on the metal in both NaCl and HCl. This observation is likely due to the formation of salts of gallium in the chloride environment[89]. This observation makes it difficult (and perhaps inappropriate) to compare the results from Figure 6 with those from Figure 2 since the electrochemical mechanisms appear different. Figure 7 shows the black shell that forms when anodically polarizing EGaIn in hydrochloric acid or sodium chloride salt solution. These salts may be present at lower anodizing voltages, but may not be apparent to the naked eye since they will be thinner.

After the drop falls, the black shell slowly dissolves, suggesting it is not stable (e.g., gallium chloride dissolves in water). In acidic solution, this black shell dissolves faster than in NaCl solution. We are presently exploring alternative electrolytes that have greater electrochemical stability than chloride ions.

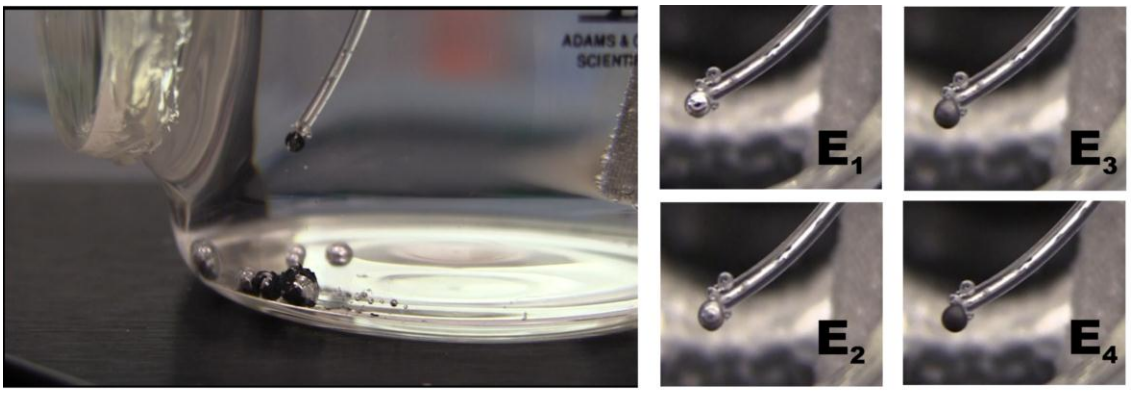


**Figure 7.** Black shell formation on EGaIn in HCl and NaCl solution under oxidative conditions. As the applied voltage increases ($E_1$ to $E_4$) the shell gets darker as shown in the smaller inset images at the right. Here $E_1$ is equal to -1 V and $E_4$ is equal to ~ 1.5 V.

## 5.5 Mathematical analysis

The goal of this work is to use an amperometric technique to detect oxidation events. The measured currents reported in this chapter could, in principle, contain contributions from both faradic current and non faradic current, but faradic current provides the most insight into the oxidation process. Although we believe that the spikes in current are primarily due to oxidation (due to the long time scales associated with their decay, whereas capacitive currents typically have rapid decays), we sought to develop a few simple mathematical analyses to help explain the sources of the current. The models do not provide definitive answers, but do suggest possible mechanisms. As a starting point, we assume that any Faradic current due to oxidation will be proportional to surface area (A) of exposed metal,

$$I \sim A$$

The area of the drop is related to its volume. Given a constant flow rate, we can estimate the volume as a function of time using the following expression,

$$\text{Volume} \sim \text{Volumetric flow rate x time} \sim (4/3)\,\pi\, r^3 \qquad (4)$$

Here r is the radius of a drop, which scales with time as,

$$r \sim t^{1/3} \qquad (5)$$

Thus, the area is related with time as, $A \sim r^2 \sim t^{2/3}$. Finally, the anodic current for a slowly growing drop is related with time as,

$$I \sim t^{2/3} \qquad (6)$$

We fit a few current-time traces using this scaling approximation, as shown in Figure 8. Figure 8 is generated by zooming into a representative time span of a drop (specifically,

between 3000-3400 s from the data in Figure 2). The red lines capture the nature of the initial decaying peak. This line is also extended without considering the small decaying peaks. Then we subtracted the data in between red line and original data of the smaller peaks over the entire time span and generate the equation of the green lines which is the best fit of the current for these plots. The data that remains (i.e., represented by green line), which represents the slow growth of the droplet, is fit using equation (6). All the generated equations are shown in the individual plots and the $R^2$ values provides an estimate of the accuracy of the trend line. The scaling equation is based on complete surface coverage of the passive layer and assumes that the anodic current is dependent on the shape of the drop as well as time. Based on these assumptions, the generated trends (i.e., the red and green line) capture the experimental trends well. Although this model seems promising, we have observed current traces that do not always follow these trends, for which we do not presently have an explanation.

We used an additional approach to analyze the current that also assume that oxidative current should be proportional to surface area. Developing a relationship between surface area and current is important for estimating the amount of skin that ruptures. The following section seeks to develop a simple estimate to correlate the current with the exposed surface area. We analyze data taken at 0 V (i.e., Figure 2) because these conditions represent those most likely to be used outside of an electrochemical cell (e.g., in a rheometer or in a microfluidic channel).

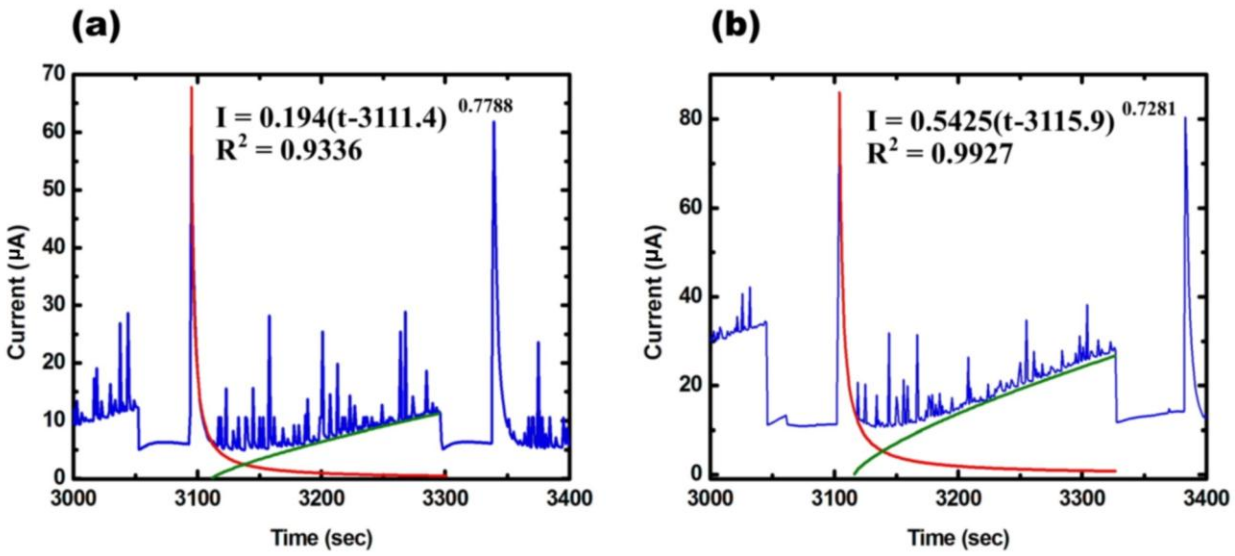


**Figure 8.** Mathematical fit of the anodic current traces for a drop that has a lifetime in between 3100 to 3300 s. a) Scaling analysis for EGaIn when it flows at 200μl/hr and applied voltage is fixed at 0 V. The anodic current varies with time as $t^{0.77}$. b) Scaling analysis for EGaIn when it has the same flow rate but the potential is fixed at 0.1 V. The anodic current varies with time as $t^{0.72}$.

The large spikes shown in Figure 2 occur when the drops suddenly emerge from the tube. This peak exhibits an anodic current of 70 μA. The amount of charge associated with this peak (0.000617 micro coulombs, μC) can be calculated by integrating (i.e., numerical integration by trapezoidal rule) the current over the first 25 s of its decay. The radius of the drop as it pops out of the tube can be estimated by the duration of the delay time between drops. During the time delay (~60 s) between the time a drop falls and a new drop forms, the syringe pump continues to displace metal. The volume displaced by the pump during this time corresponds to a drop radius of $\sim\left(\frac{60x200x3}{4x\pi x3600}\right)^{1/3}$ ~ 0.93 mm. Here, the flow rate of egain is 200μl/hr and 3600 is the conversion factor of an hour to seconds. Given this value,

the change in anodic current per unit change in area is ~ ( 70μA/ ($4\pi r^2$)) ~ 6.5 μA/$mm^2$ and the amount of charge associated with this area is $5.68x10^{-5}$ μC/$mm^2$.

As the droplet grows, we observe additional sharp peaks that are smaller and shorter in duration than the initial peak. We assume that these small peaks are due to the oxide rupturing to expose a small amount of fresh metal. Between 23 to 25 small decaying peaks occur during the life time of a drop. These peaks are expected to be smaller than the initial peak since the initial peak is associated with exposure of a larger amount of fresh metal.

If the drop shape is nearly spherical, then the radius of the drop at the end of this life time (i.e., just before falling) is

$$\sim \left(\frac{3x11.11}{4x\pi}\right)^{1/3} \sim 1.38 \text{ mm}$$

The smaller peaks are not apparent until the first large peak decays sufficiently (~25 s, or $t_2$ in Figure 9). The change in surface area due to each small peak can be estimated by the following formula: surface area of the drop at the end of the drop life time minus surface area of the drop corresponds to initial drop shape.

~ ($(4\pi(1.38)^2$)-( ($4\pi(0.93)^2$)) ~ 13.06 $mm^2$ .

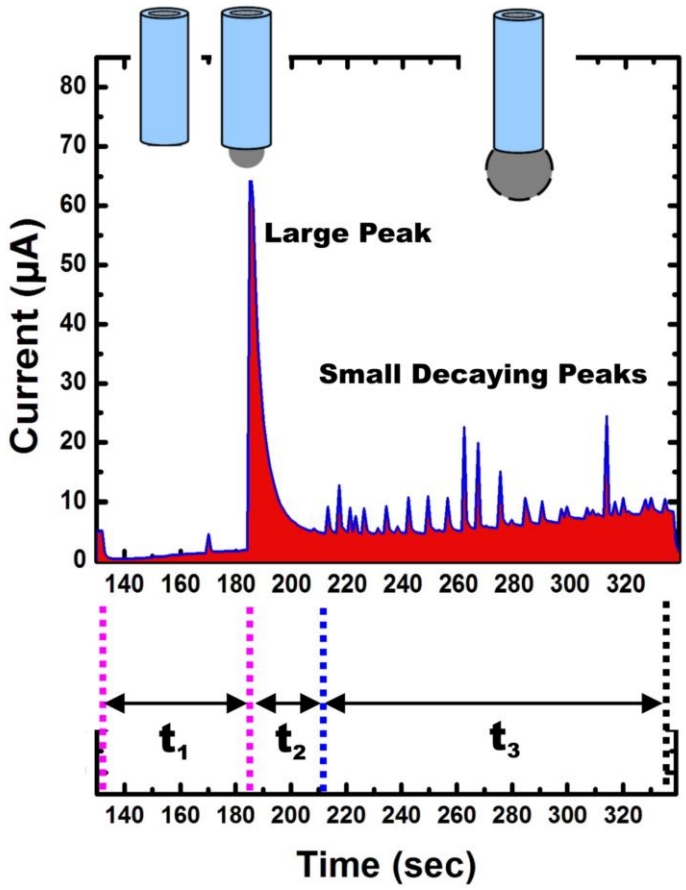


**Figure 9**: Mathematical analysis from drop shape, current and time data for a drop that spans between 130 to 340 s. The anodic current shows a large peak as the drop pops out of the tube. A number of small decaying peaks are observed afterward until the drop falls. This analysis is for 200μl/hr egain flow rate and the applied potential is fixed at 0 V (i.e., the data from Figure 2). We define $t_1$, $t_2$ and $t_3$ as the time taken by the drop to pop out of the tube (i.e., 60 s) , time for the large peak to decay (i.e, 25 s) and time scale of getting small decaying peaks (i.e., 175 s). The area under the baseline of smaller peaks is subtracted from the total charge as indicated by red area below the blue anodic current traces. The charge associated with per unite change in area (i.e, $5.6 \times 10^{-5}$ μC/mm$^2$) is found to be equal and independent of the peak nature (i.e., large or small). This suggests the total nature of the current is due to the oxide skin rupturing.

To calculate the amount of area exposed per peak, we use the final drop size and divide the change in surface area over time by the number of peaks. For 200μl/hr EGaIn at 0 V, each

drop has a life time of 200 s. If the flow of egain is perfectly continuous then after 200 s, nearly ~ 200s x 200μl/3600s ~ 11.11μl ~ 11.11$mm^3$ of EGain will have been extruded. We already found the radius of the drop at the end of this life time (i.e., just before falling) is 1.38mm. Therefore, the change in surface area is 23.9 $mm^2$-10.9 $mm^2$ = 13 $mm^2$. There are approximately 25 peaks during this time period, so each peak, on average, should correspond to 0.52 $mm^2$ area being exposed. The charge associated with the small peaks can be found by integrating the current over time as well. In order to find the exact amount of charge associated with these small peaks, we have subtracted the associated charge below the base line current (i.e., area under the base line for small peaks). Finally, we found the associated charge density with this each of the small peaks was 5.59x$10^{-5}$ μC/ $mm^2$ ( i.e., charge per peak/ change in area per small peak).

This finding –that is, that the charge per area for the initial spike is nearly identical to the charge per area for the smaller spikes – implies several compelling results with our stated hypothesis: i) Current relates with exposed surface area. ii) Charge per unit of surface area is the same, irrespective of large or small peaks. iii) Overall current may be due to oxidation of the surface and it increases with time as the droplet shape increases.

## 5.6 Effect of dissolved oxygen

All of the experiments reported to this point were carried out mostly in water that was not degassed; that is, it contains oxygen, which in principle, can react with Ga to form gallium

oxide. To elucidate the effect of dissolved oxygen on the oxidation of liquid metal during this analysis, we carried out two experiments; one in oxygenated water and another one in under nitrogen (deoxygenated water). To remove the dissolved oxygen from deionized water, we bubbled nitrogen gas in DI water for an hour and purged nitrogen gas above the water in the electrochemical cell during the experiments. A syringe pump injected EGaIn at 50 μl/hr and 0 V. Figure 10a shows the results; the overall trends of this plot are very similar to those from the identical experiment performed without purging (c.f Figure 10c), which suggests that dissolved oxygen plays a minimum role in the measurements. There are few other notable differences: The anodic current is greater by a factor of 1.5 in deionized water (without nitrogen gas bubbling); this result could be explained by the differences in conductivity of DI water with dissolved gas relative to purged DI water[90]. Also, the frequency of the drops decreases inexplicably in Figure 10a (4 drops in 100 min) relative to Figure 10c (6 drops in 100 min). The small peaks decay over 0.3-0.6 s ( in Figure 10b) which is longer than the decay observed in Figure 10d which is 0.08 to 0.1 s.

During these measurements , we extruded EGaIn at 50μl/hr which is 4 times slower than our earlier experiments at 200μl/hr and fixed the applied potential at 0 V (vs Ag/AgCl reference electrode).The potentiostat records the anodic current every 0.01 s (i.e., two orders of magnitude faster than the 200μl/hr data). Compared to 200μl/hr at 0 V (c.f. Figure 2), there are quite a few differences observed in the measured data in Figure 10. Lowering the flow rate should have increased in the lull time between drops , but there was no lull between two drops. The droplet came out of the tube as soon as it fell down without any delay. Notably,

we performed these experiments after refilling the syringe and tube with metal. It is probable that the sample preparation resulted in no bubbles, whereas previous measurements (c.f., Figure 2) had trapped air in the lines. As a result droplet comes out continuously without any lull. This observation led us to re-evaluate the lull time between drops in the 200µl/hr data (c.f., Figure 2).

We assumed the compression of trapped air (or bulging of the tube) caused the lull time in the 200 µl/hr data. Volumetric displacement by the syringe pump should cause trapped air in the lines to compress until it reaches a critical pressure necessary to rupture the oxide skin. A simple mathematical analysis shows that this explanation is reasonable. We find that 1% change in volume of the air (i.e., $\frac{V_2}{V_1} = \frac{P_1}{P_2} = \frac{P_1}{P_1 + P_C} = \frac{\boldsymbol{101.325}}{\boldsymbol{101.325 + 1}} \sim \boldsymbol{0.99}$, or change of 1%) can induce the metal to flow inside the tube. Here, $P_1$ is the initial pressure, $P_2$ is the final pressure and $P_c$ is the critical pressure to flow egain through a tube with a 500 micron inner diameter. We calculate $P_c$ using the Young Laplace equation[3]. The lull time between drops for the 200µl/hr data was approximately 1 min and during this time 3.33 $mm^3$ of EGaIn should have been extruded from the syringe. Since the change in volume is 3.33 $mm^3$ (i.e, $V_1$-$V_2$ = 3.33 $mm^3$), the initial volume of air (i.e., the volume of the air pocket) should be approximately 333 $mm^3$. The pocket of air must be in the tube or syringe. If the flexible tube does not bulge then the length of tube that corresponds to this air volume is equal to 1698 mm which is unreasonable considering the tube is less than a meter long. If the air is trapped inside the syringe, which has a 4.7 mm diameter, then the length corresponding to this volume of air is 192 µm, which is reasonable. Based on this analysis, we believe the 50µl/hr

data (Figure 10) did not exhibit any lull in between drops because it lacked air inside the tube, i.e., the metal was extruding continuously without any trapped air.

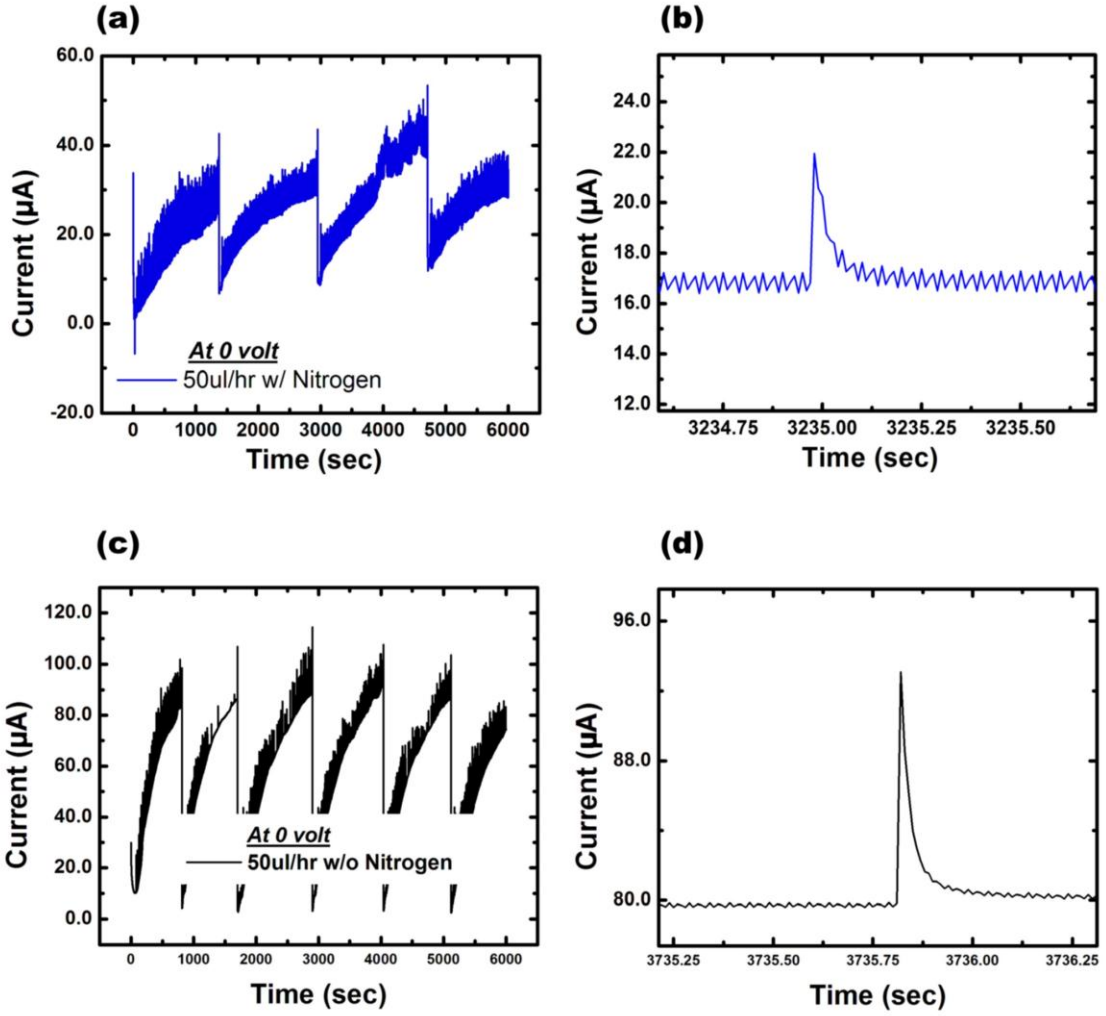


**Figure 10**: Amperometric analysis of EGaIn for slower flow rate. EGaIn is extruded at 50μl/hr and the applied potential is fixed at 0 V. a) Anodic current traces of EGaIn in deionized water with nitrogen purging. Here the anodic current shows smaller magnitude in compare with (c) because of decrease in conductivity of water[90] . Approximately 4 drops are found here with no large peak and no lull period as well. b) The nature of one small peak in 1 s scale is shown. This peak decays within 0.3 s. It is still faster than the decay time in 200μlhr but slower than what we found in (d). c) Anodic current traces of EGaIn in deionized water

without nitrogen purging. Approximately 6 drops are found. In compared with Figure 2, the anodic current shows an increasing trend with no large decay and no lull between the drops. A number of small decaying peaks are only found. d) Capturing the nature of one small decaying peak in 1 s scale. It decays in ~0.1 s which is much faster than the decay time of smaller peaks in 200µl/hr.

## 5.7 Conclusion

In this chapter we demonstrated, for the first time, an amperometric technique to measure the formation of an oxide skin that occurs upon rupture of an anodic film on EGaIn. A syringe pump extrudes EGaIn in a controlled manner into water to produce fresh metal surface at a known rate. Amperometry detects the real time rupture and oxidation of the surface under anodic polarization of the metal. Our primary goal was to prove the feasibility of this technique, explore the parameter space, and take the first steps toward analyzing the data using this approach. The presence of multiple current spikes suggests that the technique is indeed capable of detecting the rupture of the oxide skin. The anodic current exhibits some sharp peaks that decay when the metal is polarized in a potential range that is more positive than its standard electrode potential but less than the potential of water electrolysis (i.e., greater than -0.52 volt and less than 1.5 volt). Several smaller peaks are also observed as the droplet grows bigger, which is in good agreement with our hypothesis. Both capacitive and faradic current could contribute to the overall anodic current, although the time scales involved in the decay of peaks suggests oxidation.

The anodic current exhibits similar trends in both acidic and neutral salt electrolytes, but different from that observed in DI Water. The formation of a black shell around the drop of EGaIn suggests a different mechanism occurs than that observed in DI water. The black shell grows thicker with increasing positive voltage. Analogously, if the oxide skin can be grown thicker electrochemically then it may be possible to tune the critical yield stress of the liquid metal using anodization. This property may be useful in applications in which the metal is designed to flow in response to pressure (e.g., the applications described in **Chapters 2** and **3**).

We found that the presence of oxygen does not impact the phenomenological behavior of the amperometric measurements, although it does increase the magnitude of the current, possibly due to increased conductivity of the water.

We have also done some preliminary mathematical analyses of the data. The change in baselines current (at 0 and 0.1 V) is in good agreement with a simple model that accounts for changes in the surface area of the metal. We found the associated charge per unit change in surface area is $5.6 \times 10^{-5}$ $\mu C/mm^2$ regardless of the size of the peaks.

This analysis, in the future, will be linked together with an in situ rheological study to measure and detect the rupture of the oxide and correlate this behavior with changes to mechanical properties of the oxide skin. The metal will be stressed under a rheometer to measure the mechanical stability of the surface of the composite and as soon as the metal

surface gets ruptured the anodic current will be detected electrochemically due to a sharp peak. Using this novel approach, the surface of the composite will be tuned, the modified yield stress will be measured and finally, the rupture of the surface will be detected electrochemically.

## References


[1] Allen J. Bard and Larry R. Faulkner, *Electrochemical Methods: Fundamentals and Applications*, 2nd ed. (John Wiley and Sons,Inc., 2001).

[2] S. J. French, D. J.Saunders, and G. W.Ingle, The Journal of Physical Chemistry **42** (2), 265 (1937).

[3] Michael D. Dickey, Ryan C. Chiechi, Ryan J. Larsen *et al.*, Advanced Functional Materials **18** (7), 1097 (2008).

[4] M. J. Regan, H. Tostmann, P. S. Pershan *et al.*, Physical Review B **55** (16), 10786 (1997).

[5] R. J. Larsen, M. D. Dickey, G. M. Whitesides *et al.*, Journal of Rheology **53** (6), 1305 (2009).

[6] J. H. So, J. Thelen, A. Qusba *et al.*, Advanced Functional Materials **19** (22), 3632 (2009).

[7] M. R. Khan, G. J. Hayes, J. H. So *et al.*, Applied Physics Letters **99** (1), 013501 (2011).

[8] Harvey B. Herman and Allen J. Bard, Analytical Chemistry **36** (3), 510 (1964).

[9] Harvey B. Herman and Allen J. Bard, Analytical Chemistry **36** (4), 971 (1964).

[10] T. Gueshi, K. Tokuda, and H. Matsuda, Journal of Electroanalytical Chemistry **89** (2), 247 (1978).

[11] M. D. Hawley and S. W. Feldberg, The Journal of Physical Chemistry **70** (11), 3459 (1966).

[12] H. B. Herman and A. J. Bard, Analytical Chemistry **35** (9), 1121 (1963).

[13] Karl Heinz Lubert and Kurt Kalcher, Electroanalysis **22** (17-18), 1937 (2010).

[14] Peter T. Kissinger and William R. Heineman, Journal of Chemical Education **60** (9) (1983).

[15] R. P. Baldwin, K. Ravichandran, and R. K. Johnson, Journal of Chemical Education **61** (9), 820 (1984).

[16] T. R. Beck, Electrochimica Acta **18** (11), 807 (1973).

[17] T. R. Beck, Electrochimica Acta **18** (11), 815 (1973).

[18] A. K. Vasudeven, K. Sadananda, and N. Louat, Materials Science and Engineering: A **188** (1-2), 1 (1994).

[19] J. G. Hines, Corrosion Science **1** (1-2), 21 (1961).

[20] G. T. Burstein and R. J. Cinderey, Corrosion Science **32** (11), 1195 (1991).

[21] P. D. Bastek, R. C. Newman, and R. G. Kelly, Journal of the Electrochemical Society **140** (7), 1884 (1993).

[22] Pierre R. Roberge, *Corrosion Engineering: Principles and Practice*. (McGraw-Hill, 2008).

[23] Tamás Pajkossy, Journal of Electroanalytical Chemistry and Interfacial Electrochemistry **300** (1-2), 1 (1991).

[24] Tamás Pajkossy and Lajos Nyikos, Electrochimica Acta **34** (2), 171 (1989).

[25] Tamás Pajkossy and Lajos Nyikos, Electrochimica Acta **34** (2), 181 (1989).

[26] A. Imre, T. Pajkossy, and L. Nyikos, Acta Metallurgica et Materialia **40** (8), 1819 (1992).

[27] L. Nyikos and T. Pajkossy, Electrochimica Acta **31** (10), 1347 (1986).

[28] L. Nyikos, T. Pajkossy, A. P. Borosy *et al.*, Electrochimica Acta **35** (9), 1423 (1990).

[29] A. P. Borosy, L. Nyikos, and T. Pajkossy, Electrochimica Acta **36** (1), 163 (1991).

[30] I. A. Bagotskaya and V. E. Kazarinov, Journal of Serb Chemical Society **57** (12) (1992).

[31] M. Metikos-Hukovic, R. Babic, and S. Omanovic, Journal of Electroanalytical Chemistry **374** (1-2), 199 (1994).

[32] N. Cabrera and N. F Mott, Reports on Progress in Physics **12** (1), 163 (1949).

[33] L. Young, *Anodic Oxide Films*. (Academic Press, NY, 1961).

[34] S. Ikonopisov, Electrochimica Acta **22** (10), 1077 (1977).

[35] L. Kiss, Russian Journal of Electrochemistry **36** (10), 1051 (2000).

[36] T. Hurlen, C. Simon, W. Wilhelmsen *et al.*, Electrochimica Acta **34** (4), 519 (1989).

[37] M. Philippe, *Corrosion Mechanism in Theory and Practice*, 2nd ed. (Marcel Dekker Inc, NY, 2002).

[38] D. D. Macdonald, Pure Appl. Chemisty **71** (6) (1999).

[39] M. M. Lohrengel, Materials Science & Engineering R-Reports **11** (6), 243 (1993).

[40] R. S. Alwitt, Journal of The Electrochemical Society **114** (8), 843 (1967).

[41] J. W. Diggle, Thomas C. Downie, and C. W. Goulding, Chemical Reviews **69** (3), 365 (1969).

[42] H. J. W. Lenderink, M. V. D. Linden, and J. H. W. De Wit, Electrochimica Acta **38** (14), 1989 (1993).

[43] Joong-do Kim and Su-il Pyun, Electrochimica Acta **40** (12), 1863 (1995).

[44] W. C. Moshier, G. D. Davis, and J. S. Ahearn, Corrosion Science **27** (8), 785 (1987).

[45] A. W. Hassel and M. M. Lohrengel, Electrochimica Acta **40** (4), 433 (1995).

[46] D. Gong, C. A. Grimes, O. K. Varghese *et al.*, Journal of Material Researach **16** (12), 3331 (2001).

[47] T. R. Beck, Journal of the Electrochemical Society **115** (9), 890 (1968).

[48] J. Pan, D. Thierry, and C. Leygraf, Electrochimica Acta **41** (7-8), 1143.

[49] G. T. Burstein and P. I. Marshall, Corrosion Science **23** (2), 125 (1983).

[50] T. P. Hoar and J. C. Scully, Journal of The Electrochemical Society **111** (3), 348 (1964).

[51] T. Hagyard and J.R. Williams, Trans. Faraday Soc. **57**, 2288 (1961).

[52] G. T. Burstein and R. C. Newman, Electrochimica Acta **25** (8), 1009 (1980).

[53] J. J. Podesta, G. P. Rothwell, and T. P. Hoar, Corrosion Science **11** (4), 241 (1971).

[54] F. P. Ford, G. T. Burstein, and T. P. Hoar, Journal of The Electrochemical Society **127** (6), 1325 (1980).

[55] N. D. Tomashov and L. P. Vershinina, Electrochimica Acta **15** (4), 501 (1970).

[56] T. N. Anderson, J. L. Anderson, and H. Eyring, The Journal of Physical Chemistry **73** (11), 3562 (1969).

[57] T. Hagyard and W. B. Earl, Journal of The Electrochemical Society **114** (7), 694 (1967).

[58] G. S. Frankel, C. V. Jahnes, V. Brusic *et al.*, Journal of The Electrochemical Society **142** (7), 2290 (1995).

[59] G. S. Frankel, B. M. Rush, C. V. Jahnes *et al.*, Journal of The Electrochemical Society **138** (2), 643 (1991).

[60] R. P. Wei, M. Gao, and P. Y. Xu, Journal of The Electrochemical Society **136** (6), 1835 (1989).

[61] J. H. Christie and R. A. Osteryoung, Journal of Electroanalytical Chemistry and Interfacial Electrochemistry **49** (2), 301 (1974).

[62] James J. Lingane and I. M. Kolthoff, Journal of the American Chemical Society **61** (4), 825 (1939).

[63] James J. Lingane and I. M. Kolthoff, Journal of the American Chemical Society **61** (5), 1045 (1939).

[64] James J. Lingane and Brian A. Loveridge, Journal of the American Chemical Society **66** (9), 1425 (1944).

[65] R. S. Nicholson and Irving Shain, Analytical Chemistry **36** (4), 706 (1964).

[66] P. Surmann and H. Zeyat, Analytical and Bioanalytical Chemistry **383** (6), 1009 (2005).

[67] C. Wei, A.J. Bard, I. Kapui *et al.*, Analytical Chemistry **68** (15), 2651 (1996).

[68] P. A. Giguere and D. Lamontagne, Science **120** (3114), 390 (1954).

[69] T. Hurlen, Electrochimica Acta **9** (11), 1449 (1964).

[70] R. D. Armstrong, W. P. Race, and H. R. Thirsk, Journal of Electroanalytical Chemistry and Interfacial Electrochemistry **31** (2), 405 (1971).

[71] N. Horasawa, H. Nakajima, S. Takahashi *et al.*, Dental Materials Journal **16** (2), 200 (1997).

[72] I. A. Bagotskaya, A. M. Morozov, and N. B. Grigoryev, Electrochimica Acta **13** (1968).

[73] A. Frumkin, N. Polianovskaya, N. Grigoryev *et al.*, Electrochimica Acta **10** (1965).

[74] R. S. Perkins, Journal of Electrochemical Society **119** (6), 713 (1972).

[75] R. S. Perkins, Journal of Electroanalytical Chemistry **101** (1979).

[76] A. Varadharaj and G. P. Rao, Proc. Indian Acad. Sci. (Chem. Sci.) **102** (2), 177 (1990).

[77] T. Hurlen, T. Valand, and G. Lunde, Electrochimica Acta **9**, 1433 (1964).

[78] S. J. Duncan and G. T. Burstein, Journal of Applied Electrochemistry **17** (1), 196 (1987).

[79] S. B. Saidman and J. B. Bessone, Electrochimica Acta **36** (14), 2063 (1991).

[80] H. Zhou, M. Xu, Q. Huang *et al.*, Journal of Applied Electrochemistry **39** (10), 1739 (2009).

[81] B. Miller and R. E. Visco, Journal of The Electrochemical Society **115** (3), 251 (1968).

[82] R. Piercy and N. A. Hampson, Journal of Applied Electrochemistry **5** (1), 1 (1975).

[83] M. Metikos-Hukovic and S. Omanovic, Journal of Electroanalytical Chemistry **455** (1-2), 181 (1998).

[84] S. Omanovic and M. Metikos-Hukovic, Thin Solid Films **266** (1), 31 (1995).

[85] R. D. Armstrong, A. B. Suttie, and H. R. Thirsk, Electrochimica Acta **13** (1), 1 (1968).

[86] J. N. Butler and M. L. Meehan, Journal of Physical Chemistry **70** (11), 3582 (1966).

[87] M. Pourbaix, *Atlas of Electrochemical Equilibria in Aqueous Solutions—Gallium.* (National Association of Corrosion Engineers, Houston, Texas, 1974).

[88] V. V. Losev, *Standard Potentials in Aqueous Solutions*. (Marcel Dekker Inc, NY, USA, 1985).

[89] Taisiya I. Popova, Irina A. Bagotskaya, and Edward D. Moorhead, *Encyclopedia of Electrochemistry of the Elements*. (Marcel Dekker, Inc., New York, 1978).

[90] M. J. Francis, Journal of Physical Chemistry C **112** (2008).